Influence of the dipolar interaction on phase diagram, magnons, and magnetization in quasi-one-dimensional antiferromagnets on a hexagonal lattice

M. Hummel and F. Schwabl
Physik-Department, Technische Universität München, D-85747 Garching, Germany

C. Pich
Physics Department, University of California, Santa Cruz, California 95064
(Received 30 December 1999; published 13 February 2001)

The role of the dipole-dipole interaction in quasi-one-dimensional antiferromagnets is investigated within a Heisenberg model with nearest-neighbor exchange. We deal with systems in which the magnetic ions are located on a hexagonal lattice, i.e., frustration is present when three-dimensional order sets in. We perform a ground-state calculation for different ratios of dipolar energy to interchain-exchange energy and find several commensurate and incommensurate phases. This is a consequence of the competing character of these two interactions. For the commensurate phases the influence of fluctuations is studied by means of linear spin-wave theory. It turns out that all commensurate phases are stable against fluctuations. The theoretical spin-wave spectra are compared with experiments on $CsMnBr_3$ and $RbMnBr_3$. The results suggest that the most important source of anisotropy in these Mn compounds is the dipole-dipole interaction. Furthermore the magnetic phase-diagram for small dipolar energies is investigated. A spin-wave calculation allows one to calculate the influence of the fluctuations on physical properties like ground-state energy and magnetization. These results compare favorably with measurements on $CsMnBr_3$.

DOI: 10.1103/PhysRevB.63.094425 PACS number(s): 75.10.Jm, 75.30.Ds, 75.30.Gw, 75.50.Ee

I. INTRODUCTION

The interest in unconventional magnetic systems has been renewed in the last few years.[1] Competing interactions as well as geometric frustration due to the underlying lattice can lead to unconventional ground states, unique phase diagrams, and novel critical phenomena.[2] The fact that the ground states in these systems are highly degenerate and because of the low dimensionality the contributions of fluctuations to physical observables are enhanced.

In real magnets the dipole-dipole inter-action (DDI) is always present in addition to the exchange interaction. Although the DDI is usually two to three orders of magnitudes lower than the exchange interaction, it is nevertheless crucial to study its implications in the physics of phase transitions. Due to its anisotropic and long-range character the DDI changes the physics in the critical region qualitatively[3] and has also a drastic influence on ground states and excitation spectra[4,5] especially in low-dimensional systems.

In this work we particularly study the influence of the DDI on quasi-one-dimensional antiferromagnetic spin systems on a hexagonal lattice. In these compounds the exchange interaction along single chains (intrachain-interaction) is several orders of magnitude larger than the interaction between different chains (interchain-interaction). The intrachain as well as the interchain interaction are antiferromagnetic. The quasi-one-dimensionality appears due to the fact that one has direct superexchange along the chains, whereas the interaction between chains is mediated by two nonmagnetic ions.

The quasi-one-dimensional systems, which have been studied most intensively in the context of Haldane's phase,[6] solitonic excitations[7] and the effects of magnetic frustration[8] are the ternary compounds ABX_3 (A alkaline, B transition metal, and X halogen). In these systems the carrier of the magnetic moment, the B ions, are located on a hexagonal lattice,[8] leading to frustration effects when three-dimensional order sets in. We are mainly interested in the Mn compounds; due to the fact that their spin value $S=5/2$, spin-wave theory should be a good approximation. Furthermore, as the orbital angular momentum L is zero apart from small relativistic corrections and therefore the crystal-field anisotropy is only of the order of at most 20% of the dipolar energy,[9] the DDI should be the most important source of anisotropy.

The role of the dipolar interaction in ferromagnetic spin chains, which are coupled antiferromagnetically has been studied quite well.[10,4,11] For $CsNiF_3$, for example, the dipolar origin of the unexpected collinear ground state was elucidated, the spin-wave dispersion calculated in a dipolar Heisenberg model was successfully compared with the experiment and furthermore it was possible to determine a reliable value of the strength of the interchain exchange interaction.[12]

The influence of the DDI on the properties of quasi-one-dimensional antiferromagnetic spin chain systems on the other hand, has not yet been studied very thoroughly. Instead, the DDI is often replaced by a single-ion anisotropy,[13] truncated after the first term[14] or the coupling between spin chains is neglected entirely.[15] Therefore the effect of the DDI is studied in a systematic way in this paper.

The outline of the paper is as follows. In Sec. II we introduce the model, in Sec. III we calculate the ground states for the whole parameter region of the ratio of dipolar energy to interchain exchange energy without magnetic field. These ground-state investigations are supplemented by a linear spin-wave calculation in Sec. IV for the commensurate phases; in this section we also compare our findings with

 ©2001 The American Physical Society

neutron scattering measurements of the spin-wave dispersion in $CsMnBr_3$. In Sec. V we examine the magnetic phase diagram for low dipolar energies for fields both parallel and perpendicular to the chain direction. Based on these ground states we perform a spin-wave calculation and investigate the influence of fluctuations on the magnetization. We show that quantum fluctuations in our dipolar model are responsible for the huge anisotropy of the magnetization found in experiments. In Appendix A the formulas for the spin-wave spectra of the dipolar 120° structure with an applied field are given, whereas the dipolar tensor is briefly discussed in Appendix B.

II. MODEL

The Hamiltonian of the dipolar antiferromagnet without applied field reads

$$H=-\sum_{l\neq l'}\sum_{\alpha\beta}(J_{ll'}\delta^{\alpha\beta}+A_{ll'}^{\alpha\beta})S_l^{\alpha}S_{l'}^{\beta}, \tag{1}$$

with spins $\mathbf{S}_l$ at hexagonal lattice sites $\mathbf{x}_l$. The first term describes the exchange interaction $J_{ll'}$ which includes the intrachain as well as the interchain interaction. In the following we consider only nearest-neighbor exchange, i.e.,

$$J_{ll'}=\begin{cases}-J & l,l' \quad \text{along the chains,}\\ -J' & l,l' \quad \text{within the basal plane.}\end{cases}$$

For a hexagonal lattice, where the sites of the magnetic ions are indexed by $\mathbf{x}_l=a(l+m/2,\sqrt{3}/2\cdot m,c/a\cdot n)$ with l,m,n integer, the Fourier transform of the exchange energy is given by

$$J_{\mathbf{q}}=-2J\cos q_z-2J'\left[\cos q_x+2\cos\left(\frac{q_x}{2}\right)\cos\left(\frac{\sqrt{3}}{2}q_y\right)\right]. \tag{2}$$

Here and in the following we measure wave vectors in chain direction in units of $1/c$, and wave vectors within the basal planes in units of $1/a$.

The second term in Eq. (1) is the classical dipole-dipole interaction

$$A_{ll'}^{\alpha\beta}=-G\left(\frac{\delta_{\alpha\beta}}{|\mathbf{x}_l-\mathbf{x}_{l'}|^3}-\frac{3(\mathbf{x}_l-\mathbf{x}_{l'})_{\alpha}(\mathbf{x}_l-\mathbf{x}_{l'})_{\beta}}{|\mathbf{x}_l-\mathbf{x}_{l'}|^5}\right), \tag{3}$$

where $G=1/2(g\mu_B)^2$ in cgs units. This term is evaluated by means of the Ewald summation technique,[16,17] which allows the consideration of the long-range nature of the three-dimensional DDI in terms of fast convergent sums.

III. GROUND STATES

In this section we calculate the classical ground states of the system as a function of the ratio of the dipolar energy to the interchain exchange interaction

$$\kappa'=\frac{(g\mu_B)^2}{V_zJ'}\quad , \tag{4}$$

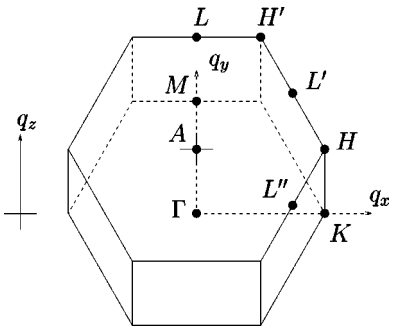

FIG. 1. Upper half of the crystallographic Brillouin zone of the hexagonal lattice. The wave vectors for the denoted points are given in Appendix C.

where $V_z=(\sqrt{3}/2)\,a^2c$ is the volume of the primitive cell of the hexagonal lattice (see Fig. 1).[18] Due to the quasi-one-dimensionality of the systems (the ratio J'/J is $10^{-2}\ldots10^{-3}$) we consider only antiferromagnetic spin configurations along the chain axis, i.e., we restrict q_z to π. The ground-state energy reads

$$E_g=-\sum_{l\neq l'}S_lM_{ll'}S_{l'}=-\sum_{\mathbf{q}}S_{\mathbf{q}}M_{\mathbf{q}}S_{-\mathbf{q}} \tag{5}$$

with

$$M_{\mathbf{q}}=\begin{pmatrix}J_{\mathbf{q}}+A_{\mathbf{q}}^{11} & A_{\mathbf{q}}^{12} & A_{\mathbf{q}}^{13}\\ A_{\mathbf{q}}^{21} & J_{\mathbf{q}}+A_{\mathbf{q}}^{22} & A_{\mathbf{q}}^{23}\\ A_{\mathbf{q}}^{31} & A_{\mathbf{q}}^{32} & J_{\mathbf{q}}+A_{\mathbf{q}}^{33}\end{pmatrix}, \tag{6}$$

where generally $A_{\mathbf{q}}^{ij}=A_{\mathbf{q}}^{ji}$ for $i\neq j$ and $A_{\mathbf{q}}^{13}=A_{\mathbf{q}}^{23}=0$ for $q_z=\pi$. The ground states are specified by those wave vectors which belong to the largest of the three eigenvalues of the matrix $M_{\mathbf{q}}$ given by

$$\lambda_1=J_{\mathbf{q}}+A_{\mathbf{q}}^{33},$$

$$\lambda_{2,3}=J_{\mathbf{q}}+\frac{1}{2}(A_{\mathbf{q}}^{11}+A_{\mathbf{q}}^{22})\pm\frac{1}{2}\sqrt{(A_{\mathbf{q}}^{11}-A_{\mathbf{q}}^{22})^2+4(A_{\mathbf{q}}^{12})^2}. \tag{7}$$

The competing quality of the exchange and dipolar interaction becomes clear in Fig. 2. If we change the relative strength of the two interactions one can see, that the wave vector minimizing the ground state energy is situated at different points of the Brillouin zone.

Particularly note the linear slope of the dipolar tensor components at the H point of the Brillouin zone. For decreasing κ' we obtain the following phases, where the actual value of J has no influence on the results, as long as $J\gg J',(g\mu_B)^2/V_z$ (the numerical values are valid for the lattice of $CsMnBr_3$,[19] i.e., $c=3.26$ Å, $a=7.61$ Å).

A. Ferromagnetic phase

$\kappa'>\kappa_1'=200.50$. In the region where the dipolar energy is large compared to the interchain exchange, the minimum of the ground-state energy is reached at the A point of the

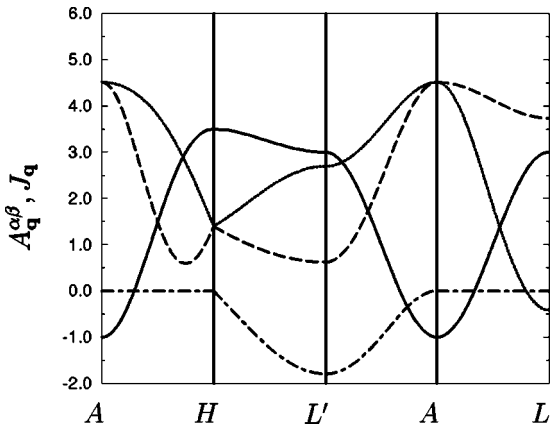

FIG. 2. Exchange interaction (solid line) and dipolar tensor for some directions in the Brillouin zone. Long-dashed: $A^{11}_{\mathbf{q}}$, dotted: $A^{22}_{\mathbf{q}}$, and dot-dashed: $A^{12}_{\mathbf{q}}$. To see the behavior of the dipolar tensor more clearly, we set $c/a=\sqrt{2/3}$. The numerical values of the dipolar tensor are given in units of G/V_z and the values for the exchange constants are set to $J=1$ and $J'=0.2$. $A^{13}_{\mathbf{q}}=A^{23}_{\mathbf{q}}=0$ for $q_z=\pi$.

Brillouin zone, i.e., at $\mathbf{q}_1=(0,0,\pi)$. This means that spins within basal planes are ordered ferromagnetically, but still antiferromagnetically along the chains.

The ground state energy is given by

$$E_g=-NS^2\left(2J-6J'+\frac{1}{2}(A^{11}_{\mathbf{q}_1}+A^{22}_{\mathbf{q}_1})\right). \tag{8}$$

Note that the dipolar components $A^{11}_{\mathbf{q}_1}$ and $A^{22}_{\mathbf{q}_1}$ have the same value. This means that the ground-state energy is the same for spin configurations where all spins are rotated within the basal plane and spins in adjacent planes are oriented antiferromagnetically [see also Goldstone mode in the spin-wave spectrum, Eq. (18)].

B. Incommensurate phase I

$\kappa_1'>\kappa'>\kappa_2'=200.12$. The ground state is an incommensurate phase in this parameter region. The wave vector moves continuously from $\mathbf{q}_1$ to the wave vector $\mathbf{q}_2=(0,2\pi/\sqrt{3},\pi)$ (see Fig. 3, Fig. 4, and thick solid line in Fig. 5) or any other path rotated by 60° (dashed lines in Fig. 5). This is due to an increase in $J_{\mathbf{q}}$ from A to L whereas $A^{\alpha\beta}_{\mathbf{q}}$ decreases.

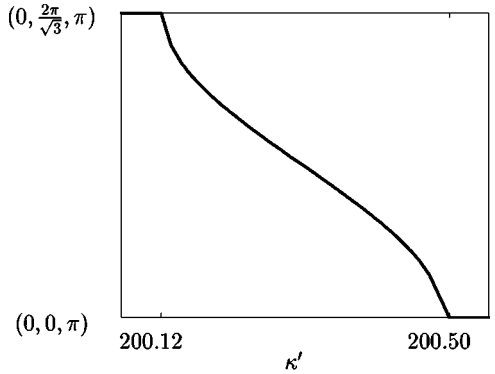

FIG. 3. Wave vector which minimizes the ground state energy in the incommensurate phase I as a function of κ'.

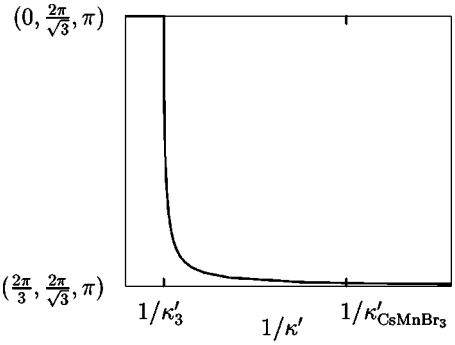

FIG. 4. Dependence of the ordering wave vector in the IC II phase on the value of κ'.

C. Collinear phase

$\kappa_2'>\kappa'>\kappa_3'=17.25$. Spins within basal planes are oriented ferromagnetically in chains, that are aligned antiferromagnetically to one another (see Fig. 6). Because of the sixfold symmetry, there are six such ground states resulting from rotation of the ferromagnetic chains. This means that the minimum of the ground state energy is reached at the points L, L' and the ones rotated by 60° in the Brillouin zone. Note that the continuous degeneracy is lifted.

The ground state energy for the domain drawn in Fig. 6 reads

$$E_g=-NS^2(2J+2J'+A^{11}_{\mathbf{q}_2}). \tag{9}$$

For a domain where the ferromagnetic chains are rotated by 60° around the z axis the ground state energy is given by

$$E_g=-NS^2(2J+2J')-\frac{1}{4}NS^2(A^{11}_{\mathbf{q}_5}+3A^{22}_{\mathbf{q}_5}-2\sqrt{3}A^{12}_{\mathbf{q}_5}), \tag{10}$$

with $\mathbf{q}_5=(\pi,\pi/\sqrt{3},\pi)$. These two ground state energies are the same, which can be shown by exact relations for the dipolar tensor components. The third domain is described by the wave vector $\mathbf{q}_6=(\pi,-\pi/\sqrt{3},\pi)$.

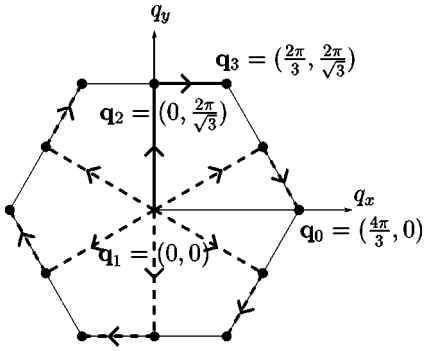

FIG. 5. Paths of the wave vector that minimize the ground-state energy in the Brillouin zone of the hexagonal lattice ($q_z=\pi$).

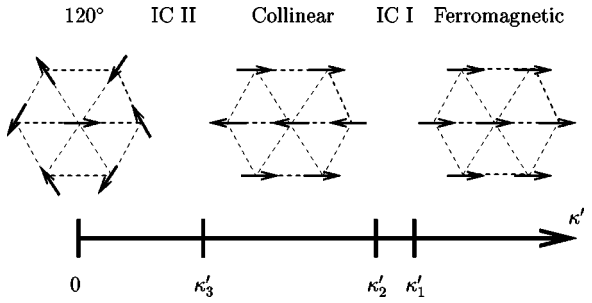

FIG. 6. Spin configurations within the basal plane for different ratios of dipolar to interchain interaction κ'. Only for $\kappa'=0$ the 120° structure is established. For infinitesimal κ' the phase IC II is favored. The spin configurations of the incommensurate phases are not sketched.

Note that if we didn't consider the IC I phase, the transition from the ferromagnetic to the collinear phase would appear at $\kappa'=200.31$, i.e., exactly between κ_1' and κ_2'. However, the ground state energy of the incommensurate phase between κ_1' and κ_2' is lower than both the one for the ferromagnetic as well as the one for the collinear phase.

D. Incommensurate phase II

$\kappa_3'>\kappa'>0$. In this incommensurate phase the wave vector moves from $\mathbf{q}_2$ to $\mathbf{q}_3=(2\pi/3,2\pi/\sqrt{3},\pi)$. The incommensurability for low dipolar energy appears because of the finite slope of the dipolar tensor at $\mathbf{q}_3$ (Ref. 11) and the parabolic behavior of the exchange energy.

The expansion of the largest eigenvalue of Eq. (7) around $(2\pi/3,2\pi/\sqrt{3},\pi)$ leads to the following ground-state energy:

$$E_g\left(\frac{2\pi}{3}-q_x,\frac{2\pi}{\sqrt{3}}-q_y,\pi\right) \approx -NS^2\left(2J+3J'-\frac{3}{4}J'(q_x^2+q_y^2) + \frac{(g\mu_B)^2}{V_z}(0.0464q_x+0.0036q_y^2)\right). \quad (11)$$

One can see that without dipolar energy (i.e., $\kappa'=0$) the lowest ground state energy is reached for $\mathbf{q}=\mathbf{q}_3=(2\pi/3,2\pi/\sqrt{3},\pi)$. However, for any infinitesimal dipolar energy the system is driven to an incommensurate ordering wave vector. The 120° phase established for vanishing dipolar energy is reached asymptotically (see Fig. 4).

E. 120° structure

$\kappa'=0$. This ground state is characterized by a three-sublattice spin configuration in each basal plane, i.e., by the wave vector $\mathbf{q}_3$ (H') and the correspondent rotated ones.

We state that for all four phases, in which the DDI is nonzero the coupling of the spin space to the real space induced by the DDI forces the spins to align within the lattice basal planes. Thus, the DDI leads to an in-plane anisotropy.

The phase diagram for the whole parameter region of κ' is shown in Fig. 6. In summary, we find three commensurate and two incommensurate phases as function of κ'.

IV. MAGNON SPECTRA

To see whether fluctuations destroy the ground states found in the previous section we perform a spin-wave calculation. To that end we write the Hamiltonian (1) in terms of creation and annihilation operators employing the Holstein-Primakoff transformation[20]

$$\tilde{S}_l^+=\sqrt{2S}f_l a_l,$$

$$\tilde{S}_l^-=\sqrt{2S}a_l^\dagger f_l,$$

$$\tilde{S}_l^z=S-a_l^\dagger a_l \quad (12)$$

with

$$f_l=\sqrt{1-\frac{a_l^\dagger a_l}{2S}} \quad (13)$$

and $S^\pm=S^x\pm iS^y$. The tilde denotes the fact that these operators have to be utilized in the rotated frame, where the local z axis is aligned in the spin direction of the classical ground state. The Fermi commutation relations for the operators (12) are satisfied if the creation and annihilation operators a and $a^\dagger$ obey Bose commutation relations. For low temperatures an expansion up to bilinear terms can be used, leading to linear spin-wave theory. The Hamiltonian then is diagonalized with a Bogoliubov transformation or the methods of Greens functions leading to the spin-wave frequencies of the system. The investigation described above is restricted to the commensurate phases, because the infinite primitive cell of the incommensurate phases resists such an analysis.

A. Ferromagnetic phase

The magnon spectrum of the ferromagnetic phase is calculated in the crystallographic Brillouin zone (see Figs. 7 and 8) The transformation to the local coordinate system reads

$$S_l^x=\sigma_l\tilde{S}_l^z,$$

$$S_l^y=\sigma_l\tilde{S}_l^x,$$

$$S_l^z=\tilde{S}_l^y, \quad (14)$$

where

$$\sigma_l=e^{i\mathbf{q}_1\mathbf{x}_l}=e^{in\pi}=\begin{cases}1 & l\in\text{plane 1 } (n=0 \bmod 2),\\ -1 & l\in\text{plane 2 } (n=1 \bmod 2)\end{cases} \quad (15)$$

mediates between the two different sublattices. After inserting Eqs. (12), (14), and (15) into the Hamiltonian (1) we obtain in linear spin-wave theory

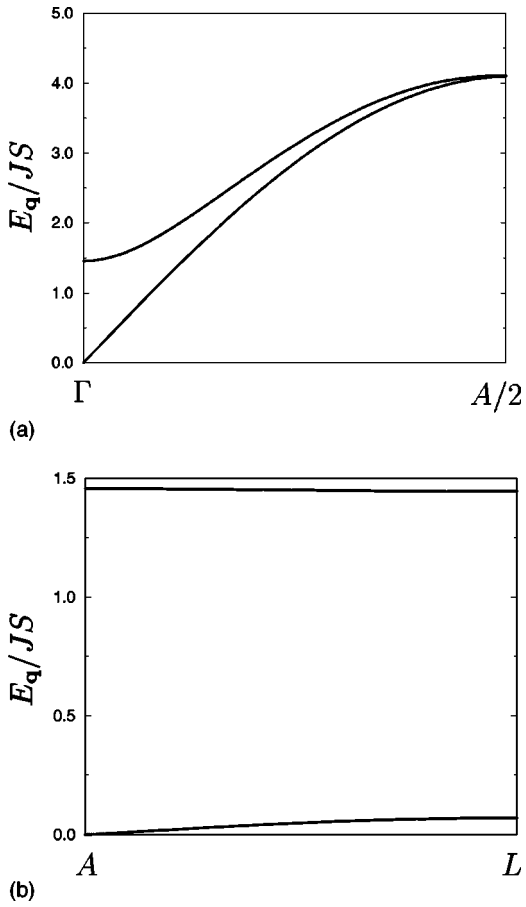

FIG. 7. Magnons of the ferromagnetic phase in the magnetic Brillouin zone. Top: in chain direction, bottom: perpendicular to it ($\kappa=10^{-2},\kappa'=10^{3}$).

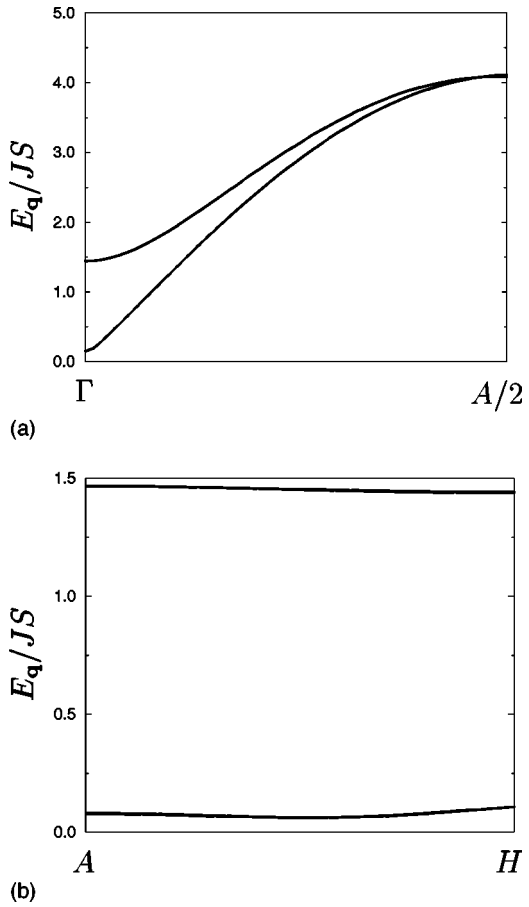

FIG. 8. Magnons in the collinear phase for $\kappa=10^{-2}$ and $\kappa'=10^{2}$. Top: Spectrum in the chain direction. Down: Spectrum in the H direction. Note the energy gap in these spectra.

$$H=E_g+\sum_{\mathbf{q}}\left\{A_{\mathbf{q}}a_{\mathbf{q}}^{\dagger}a_{\mathbf{q}}+\frac{1}{2}B_{\mathbf{q}}(a_{\mathbf{q}}a_{-\mathbf{q}}+a_{\mathbf{q}}^{\dagger}a_{-\mathbf{q}}^{\dagger})+C_{\mathbf{q}}a_{\mathbf{q}}a_{-\mathbf{q}-\mathbf{q}_1}\right.$$
$$\left.+C_{\mathbf{q}}^{*}a_{\mathbf{q}}^{\dagger}a_{-\mathbf{q}-\mathbf{q}_1}^{\dagger}+D_{\mathbf{q}}a_{\mathbf{q}}^{\dagger}a_{\mathbf{q}+\mathbf{q}_1}+D_{\mathbf{q}}^{*}a_{\mathbf{q}+\mathbf{q}_1}^{\dagger}a_{\mathbf{q}}\right\} \tag{16}$$

with

$$E_g=-NS^2(J_{\mathbf{q}_1}+A_{\mathbf{q}_1}^{11}),$$
$$A_{\mathbf{q}}=2S(J_{\mathbf{q}_1}+A_{\mathbf{q}_1}^{11})-S(J_{\mathbf{q}+\mathbf{q}_1}+A_{\mathbf{q}+\mathbf{q}_1}^{22})-S(J_{\mathbf{q}}+A_{\mathbf{q}}^{33}),$$
$$B_{\mathbf{q}}=S(J_{\mathbf{q}}+A_{\mathbf{q}}^{33})-S(J_{\mathbf{q}+\mathbf{q}_1}+A_{\mathbf{q}+\mathbf{q}_1}^{22}),$$
$$C_{\mathbf{q}}=iSA_{\mathbf{q}}^{23},$$
$$D_{\mathbf{q}}=-iSA_{\mathbf{q}}^{23}. \tag{17}$$

This quadratic Hamiltonian is diagonalized by the equations of motion for proper Greens functions[21] leading to the excitation spectrum

$$E_{\mathbf{q}}^{(1,2)}=\sqrt{\frac{1}{2}(\Omega_1\pm\Omega_2)}, \tag{18}$$

where

$$\Omega_1=A_{\mathbf{q}}^2+A_{\mathbf{q}+\mathbf{q}_1}^2-B_{\mathbf{q}}^2-B_{\mathbf{q}+\mathbf{q}_1}^2+8C_{\mathbf{q}}C_{\mathbf{q}+\mathbf{q}_1} \tag{19}$$

and

$$\Omega_2^2=(A_{\mathbf{q}}^2-B_{\mathbf{q}}^2-A_{\mathbf{q}+\mathbf{q}_1}^2+B_{\mathbf{q}+\mathbf{q}_1}^2)^2$$
$$+16\{C_{\mathbf{q}}(A_{\mathbf{q}}+B_{\mathbf{q}})-C_{\mathbf{q}+\mathbf{q}_1}(A_{\mathbf{q}+\mathbf{q}_1}+B_{\mathbf{q}+\mathbf{q}_1})\}$$
$$\times\{C_{\mathbf{q}+\mathbf{q}_1}(A_{\mathbf{q}}-B_{\mathbf{q}})-C_{\mathbf{q}}(A_{\mathbf{q}+\mathbf{q}_1}-B_{\mathbf{q}+\mathbf{q}_1})\}. \tag{20}$$

Here we changed to the magnetic Brillouin zone and therefore obtain two magnon branches.

The rotational invariance of the spins around the chain axis leads to a Goldstone mode in the spectrum. The spectrum gets unstable for $\kappa<\kappa_1'$ at infinitesimal values of q_y along the A-L direction indicating the transition to the IC I phase.

B. Collinear phase

The collinear phase of Sec. III is also stable against fluctuations. The spectrum can be calculated in analogy to the spectrum for the ferromagnetic phase; one just has to replace the ordering wave vector $\mathbf{q}_1$ by $\mathbf{q}_2=(0,2\pi/\sqrt{3},\pi)$. There is

no longer a Goldstone mode present due to the discrete degeneracy of the ground state. This is manifested in the difference of the dipolar tensor components $A^{11}_{\mathbf{q}_2}$ and $A^{22}_{\mathbf{q}_2}$.

C. 120° structure

We argued in Sec. III that the 120° structure is unstable for infinitesimal dipolar energy due to a linear slope of the dipolar tensor at the ordering wave vector. However, to gain insight in the fluctuations we performed a spin-wave calculation based on a commensurate 120°-structure, where the spins are located within the basal planes of the lattice,[22] i.e., we started with the following transformation:

$$S^x_l = \tilde{S}^x_l \sin(\mathbf{q}_0\mathbf{x}_l) + \tilde{S}^z_l \cos(\mathbf{q}_0\mathbf{x}_l),$$

$$S^y_l = \tilde{S}^x_l \cos(\mathbf{q}_0\mathbf{x}_l) - \tilde{S}^z_l \sin(\mathbf{q}_0\mathbf{x}_l),$$

$$S^z_l = \tilde{S}^y_l . \tag{21}$$

Here

$$\mathbf{q}_0\mathbf{x}_l = \frac{\pi}{c}\begin{pmatrix} 4c/3a \\ 0 \\ 1 \end{pmatrix} a \begin{pmatrix} l+m/2 \\ \sqrt{3}/2\cdot m \\ c/a\cdot n \end{pmatrix} = \frac{4\pi}{3}\left(l+\frac{m}{2}\right)+n\pi \tag{22}$$

mediates between the six sublattices. Inserting this transformation in the Hamiltonian (1) and truncating after the harmonic terms, we get a Hamiltonian with 19 different biquadratic terms (see Appendix A). This Hamiltonian is diagonalized by the equation of motion of proper Greens functions leading to a 12×12 matrix; the eigenvalues of that matrix give the energies of the spin waves. It turns out that the spin-wave spectrum is stable for weak dipolar energies, from which we conclude that this commensurate ground state is a good approximation.

The spin-wave frequencies resulting for the dipolar 120° structure for $CsMnBr_3$ are shown in Fig. 9, where we used $J=215$ GHz and $J'=0.41$ GHz respectively.[23] This leads to $\kappa'=0.774$, i.e., this substance is deep in the IC II region of the phase diagram in Fig. 6. In the experiment one observes the 120° structure; this might be caused by crystal distortions or small additional anisotropies not considered in this paper such as the spin-orbit coupling.

Including the DDI, of the three Goldstone modes only one survives reflecting the remaining rotational symmetry around the chain axis. The gaps at $\mathbf{q}=0$ are given by

$$E_{0,1} = 2S\sqrt{4J+(A^{11}_{\mathbf{q}_0}-A^{33}_{2\mathbf{q}_0})}\sqrt{\frac{9}{2}J'+\frac{1}{2}(A^{11}_{\mathbf{q}_0}-A^{11}_{3\mathbf{q}_0})}, \tag{23}$$

$$E_{0,2} = 2S\sqrt{4J+\frac{9}{2}J'+\frac{1}{2}(2A^{11}_{\mathbf{q}_0}-A^{11}_{0}-A^{11}_{2\mathbf{q}_0})}\sqrt{A^{11}_{\mathbf{q}_0}-A^{33}_{\mathbf{q}_0}}, \tag{24}$$

$$E_{0,3} = 2S\sqrt{4J+(A^{11}_{\mathbf{q}_0}-A^{11}_{2\mathbf{q}_0})}\sqrt{9J'+(A^{11}_{\mathbf{q}_0}-A^{11}_{3\mathbf{q}_0})}. \tag{25}$$

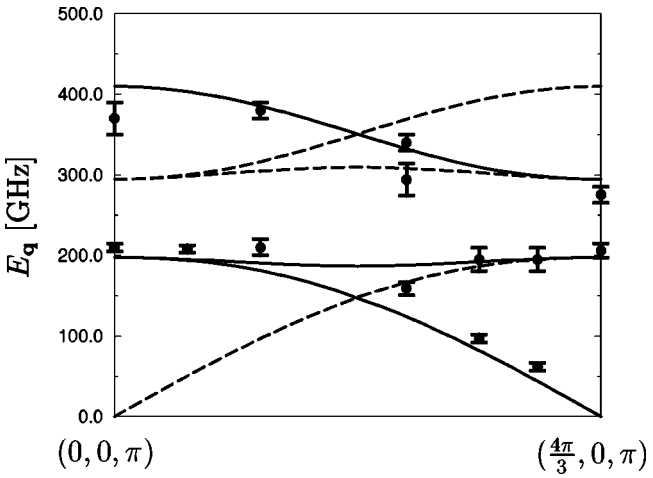

FIG. 9. Excitation energies of the 120° structure perpendicular to the chain direction. The dots are the experimental values taken from Ref. 24. The dashed and the full lines are the theoretical results, where the dashed branches cannot be seen in this scattering geometry. The full lines are the visible branches.

The spin-wave gaps at $\mathbf{q}=0$ amount to $E_{0,1}=198$ GHz, $E_{0,2}=295$ GHz, and $E_{0,3}=410$ GHz for $CsMnBr_3$, which compares favorably with the experimental values.[23,24] Note that this calculation has no free parameter to fit, since the dipolar energy is determined by the lattice constants.

In Fig. 10 we plotted the spin wave energies in the same direction as in Fig. 9 but without dipolar energy. Note that we have three zeros in the excitation energy in this case which is at variance with the measurements. Note also that the dipolar gap [Eq. (24)] which is not present without dipolar energy is larger than the gap already present without dipolar energy.

We also calculated the spin-wave gaps for $RbMnBr_3$; neglecting crystal distortions we also obtain good agreement with the experiment.[25] Thus, we do not need any single-ion anisotropy to explain these results.

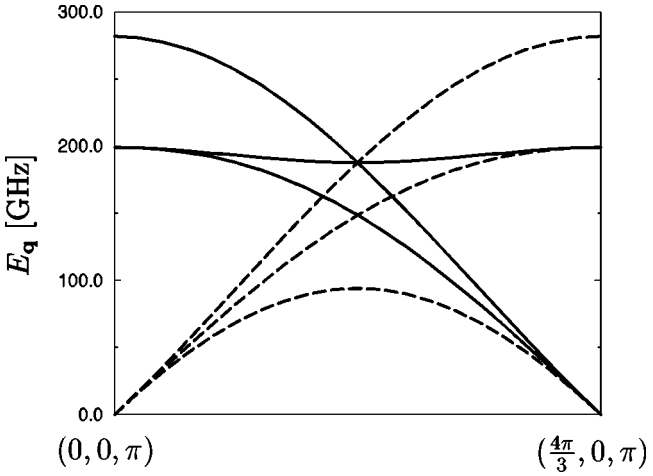

FIG. 10. Excitation energies of the 120° structure without dipolar energy. The dashed branches are the ones corresponding to the dashed ones in Fig. 9.

V. MAGNETIC PHASE DIAGRAM FOR LOW DIPOLAR ENERGY

In the last section we have shown, that the 120° structure has a stable spectrum for low dipolar energies. In this section we illuminate the influence of a magnetic field on the ground state, the magnon spectrum and the magnetization in this phase, i.e., we investigate the Hamiltonian

$$H=-\sum_{\mathbf{q}}\sum_{\alpha,\beta=1}^{3}(J_{\mathbf{q}}\delta^{\alpha\beta}+A_{\mathbf{q}}^{\alpha\beta})S_{\mathbf{q}}^{\alpha}S_{-\mathbf{q}}^{\beta}-h\sqrt{N}S_0^{z,y}, \quad (26)$$

where $h=g\mu_B H_0$. We distinguish fields along the chain direction (z) and perpendicular to that direction (y), i.e., fields applied within the basal plane. For both cases, we determine the classical ground state by energy minimization and calculate the magnon spectrum based on this ground state.

A. Field in chain direction

Numerical minimization of the classical ground-state energy under consideration of exchange energy, dipolar energy, and a magnetic field applied in chain direction shows that spins on basal-plane lattice sites are arranged on three sublattices, i.e., neighboring spins within basal planes show a phase shift of 120°. However, the applied field forces the spins to tilt in field direction by an angle φ. The ground-state energy reads

$$E_g=-NS^2(J_{\mathbf{q}_0}+A_{\mathbf{q}_0}^{11})-NS^2\sin^2\varphi[J_{\mathbf{q}_0}+A_{\mathbf{q}_0}^{11}-(J_0+A_0^{33})]. \quad (27)$$

Here φ is the angle between the basal plane and the spins, which is the same for all three sublattices. This phase is the well-known umbrella phase. Minimization of the ground state energy in Eq. (27) leads to the relation between the applied field H_0 and the tilting angle φ

$$\sin\varphi=\frac{g\mu_B H_0}{2S[J_{\mathbf{q}_0}+A_{\mathbf{q}_0}^{11}-(J_0+A_0^{33})]}. \quad (28)$$

Equation (28) reduces to the 120° phase found in the previous section for vanishing fields. For infinitesimal field the spins partially align in field direction; as already stressed, spins on different sublattices enclose the same angle with the applied field. The value of the angle increases with increasing field. At a critical field

$$H_c=\frac{1}{g\mu_B}2S[J_{\mathbf{q}_0}+A_{\mathbf{q}_0}^{11}-(J_0+A_0^{33})] \quad (29)$$

the system undergoes a phase transition to the paramagnetic phase. The phase diagram is schematically shown in Fig. 11.

The starting point for the spin-wave calculation are the proper spin variables defined in Eq. (12), which lead to fluctuations. These variables are found by performing a rotation of the spin variables given in Eq. (21) by the angle φ in chain direction

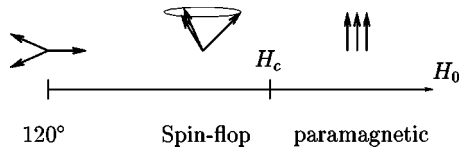

FIG. 11. Phase diagram of the 120° structure with applied field *in* the chain direction.

$$\begin{pmatrix} S_l^x \\ S_l^y \\ S_l^z \end{pmatrix}=\begin{pmatrix} \cos\varphi & 0 & -\sin\varphi \\ 0 & 1 & 0 \\ \sin\varphi & 0 & \cos\varphi \end{pmatrix} \times\begin{pmatrix} \tilde{S}_l^z\cos(\mathbf{q}_0\mathbf{x}_l)+\tilde{S}_l^x\sin(\mathbf{q}_0\mathbf{x}_l) \\ \tilde{S}_l^x\cos(\mathbf{q}_0\mathbf{x}_l)-\tilde{S}_l^z\sin(\mathbf{q}_0\mathbf{x}_l) \\ \tilde{S}_l^y \end{pmatrix}. \quad (30)$$

Note that these spin variables obey Bose commutation relations and yield to the correct classical ground state for $\tilde{S}_x=\tilde{S}_y=0$ and $\tilde{S}_z=S$, i.e., for the case without fluctuations. Inserting these operators and Eq. (12) into Eq. (26) leads to a Hamiltonian that has the same structure as the one without applied field [see Eq. (A1)] and can be diagonalized in the same way. The spectrum obtained by this calculation is shown for a special direction in Fig. 12.

In comparison to the field-free case the field lifts the degeneracy of all modes. This cannot be seen in the figure above, because the difference of the gaps is too small. The gaps for the second and third-lowest modes are $E_{\mathbf{q}=0}=197.27$ GHz and $E_{\mathbf{q}=0}=198.04$ GHz respectively, i.e., the magnetic field does not change E_0 very much [compare results from Eq. (23)], only at the Brillouin-zone boundary is the difference of the spin-wave frequencies large. However, one Goldstone mode is still present since rotational invariance around the chain axis is uneffected.

B. Field within the basal plane

1. Ground states

First of all we state, that the direction of the applied field *within* the basal plane is arbitrary for the structure of the

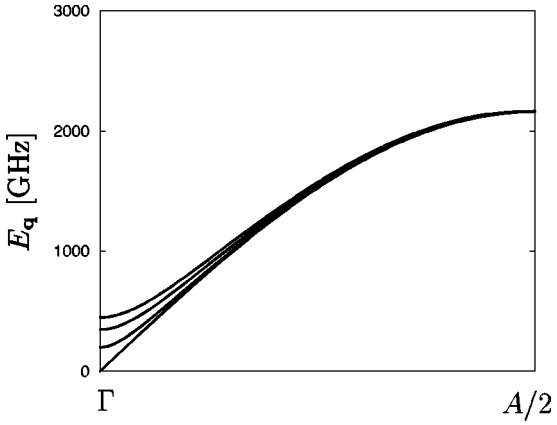

FIG. 12. Spin-wave frequencies in the chain direction in the umbrella phase for $CsMnBr_3$ for a magnetic field of 6.5 T.

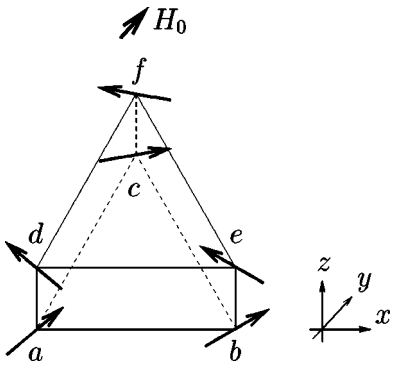

FIG. 13. General six-sublattice structure of the ground state. The direction of every spin can be described by two independent angles, the spin length is fixed. The different sublattices are denoted $a-f$ and the field is applied within the basal plane (y direction).

ground state. This is due to the fact, that the 120° ground state is rotationally invariant without applied field. In the following we will apply the field in the y direction. To find the ground state we have to minimize the classical ground state energy. This is done within a general six-sublattice system, where one has three independent sublattices in each of two adjacent basal planes (see Fig. 13).

The ground-state spin configuration of the whole magnet is built up by repetition of this basis. To describe the spatial direction of the spins, we need to know two angles for every spin (spherical coordinates), as the spin length is fixed. We formulate the ground state energy in the magnetic BZ and obtain the ground state by numerical minimization of the ground state energy.

First, we find that the spins stay *within* basal planes for realistic strengths of the dipolar energy for all values of the applied field. The dipolar energy leading to an easy-plane anisotropy in the field-free case is therefore strong enough to keep the spins within the basal plane even in the presence of a competing applied field. With this knowledge the ground state can be parametrized by six different angles, which give the direction of any spin within the basal plane. Secondly, the angles of each two adjacent spins along the chain direction (e.g., spins on sublattices a and d in Fig. 13) add up to 180° if one measures the angles with respect to the x direction. This is due to the strong antiferromagnetic exchange

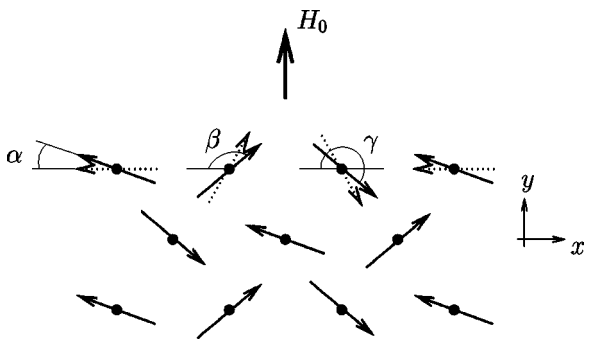

FIG. 14. Notation of the angles on the three independent sublattices in a specific basal plane.

interaction along the chains (for infinitesimal fields the spins along the chains are aligned antiferromagnetically). Therefore, the ground-state energy can be written in terms of three angles only

$$\frac{E_g}{N_g S^2} = (12J' - 4A^{11}_{0,ab})[\cos(\alpha-\beta)+\cos(\alpha-\gamma) + \cos(\beta-\gamma)] + (-4J + 2A^{11}_{0,ad}) \times [\cos(2\alpha)+2\cos(\beta+\gamma)] + \{2A^{11}_{0,ae}[\cos(2\beta)+\cos(2\gamma)+2\cos(\alpha+\beta) + 2\cos(\alpha+\gamma)] + 6A^{11}_{0,aa}\} - 2h/S(\sin\alpha+\sin\beta+\sin\gamma). \quad (31)$$

Here $N_g = N/6$, $h = g\mu_B H_0$ and α, β, γ refer to the angles of the spins to the x axis (see Fig. 14).

To find the minimum of Eq. (31) we differentiate E_g with respect to the three angles. This leads to three equations for the angles in dependence on the field. These equations cannot be solved in closed form; however, we can compute these angles to lowest order in $H_0/(8JS)$, J'/J and $(g\mu_B)^2/J'$:

$$\sin\alpha = \frac{h}{8JS}, \quad \sin\epsilon = \frac{h}{8JS(2-z)}, \quad \cos\delta = \frac{1}{2-z} \quad (32)$$

with $z = h^2/h_c^2$. The critical field to lowest order is

$$h_c^2 = \frac{48JJ'S^2}{1+\frac{1}{3J'}(A^{11}_{0,ab}-A^{11}_{0,ae})}. \quad (33)$$

Here, we have introduced the notation $\delta = \frac{1}{2}(\beta-\gamma)$ and $\epsilon = \frac{1}{2}(\beta+\gamma)$.

The qualitative behavior is as follows: As we apply an infinitesimal field, one spin (α) aligns virtually perpendicular to the applied field, whereas the other two enclose an angle of 120° and 240° with the first spin, respectively (120° structure). As the field increases α remains almost unchanged, whereas the other two angles β and γ change until they coincide at a critical field H_c for $z=1$, i.e., $\delta=0$. Above this field strength

$$\gamma = \beta \quad (34)$$

and the reorientation of the spins is like at an ordinary two-sublattice spin-flop phase. However, the angles α and β do not add up to 180° as in a simple spin-flop phase. To the lowest order the angles are given by

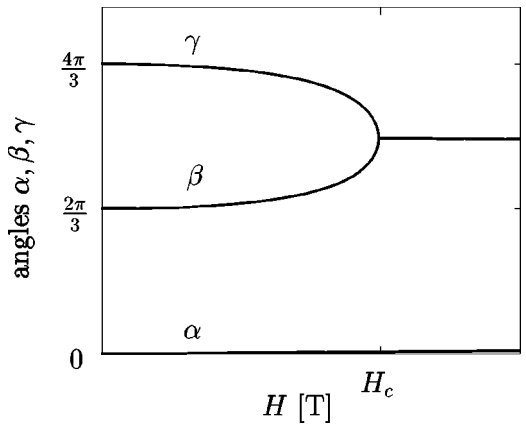

FIG. 15. The angles minimizing the classical ground state energy for $CsMnBr_3$. The critical field is $H_c = 6.35T$.

$$\sin\alpha = \frac{h}{8JS}\left(1 - \frac{3J'}{J} + \frac{1}{2J}(A^{11}_{0,ad} + 2A^{11}_{0,ab})\right)$$

$$\sin\beta = \frac{h}{8JS}\left(1 - \frac{3J'}{2J} + \frac{1}{2J}(A^{11}_{0,ad} + A^{11}_{0,ae} - A^{11}_{0,ab})\right). \tag{35}$$

These are the dipolar generalization of the results of Chubukov.[26] In Fig. 15 we have plotted the numerical results.

At $H_{\text{para}} \approx 154$ T the paramagnetic phase is reached for both a field in chain direction as well as perpendicular.

In Fig. 16 the schematic phase diagram for the 120° structure with a field applied within the basal plane is shown. Note that the dipolar energy in real materials is strong enough to keep the spins within the basal planes despite the fact that the applied field is competing. Also note, that the in-plane dipolar 120° structure is only realized for vanishing fields.

2. Magnon spectra

The magnon spectrum for the four phases of the previous section can be calculated within the crystallographic Brillouin zone. We will start from a general ground-state that can be parametrized by three angles, develop a spin-wave theory and insert the angles found by minimization of the ground-state energy.

First, we introduce

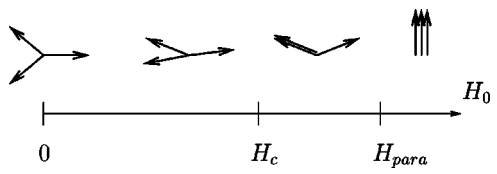

FIG. 16. Magnetic phase diagram of $CsMnBr_3$ for a field applied within the basal planes. The 120° phase is realized only for vanishing field. All spins lie in planes perpendicular to the chain direction, i.e., within the x-y planes. At H_c a phase transition occurs from a three-sublattice to a two-sublattice phase.

$$g = \exp(i\mathbf{q}_1\mathbf{x}_l) = \begin{cases} 1 & l \in \text{plane } 1 \bmod 2, \\ -1 & l \in \text{plane } 2 \bmod 2, \end{cases} \tag{36}$$

and

$$h = \frac{2}{\sqrt{3}}\sin(\mathbf{q}_4\mathbf{x}_l) = \begin{cases} 0 & l \in \text{sublattice } 1, \\ -1 & l \in \text{sublattice } 2, \\ 1 & l \in \text{sublattice } 3, \end{cases} \tag{37}$$

where $\mathbf{q}_1 = (0,0,\pi)$ and $\mathbf{q}_4 = (4\pi/3,0,0)$. Using g and h allows us to automatically depict the sublattices which are parametrized by α, β, and γ.

The spin variables in Fourier space are given by

$$\mathbf{S}_{\mathbf{q}} = \begin{pmatrix} a\tilde{S}^z_{\mathbf{q}-\mathbf{q}_1} - c(\tilde{S}^z_{\mathbf{q}-\mathbf{q}_0} + \tilde{S}^z_{\mathbf{q}+\mathbf{q}_0}) - b\tilde{S}^x_{\mathbf{q}} \\ + d(\tilde{S}^x_{\mathbf{q}-2\mathbf{q}_4} + \tilde{S}^x_{\mathbf{q}+2\mathbf{q}_4}) \\ + f(\tilde{S}^z_{\mathbf{q}+2\mathbf{q}_4} - \tilde{S}^z_{\mathbf{q}-2\mathbf{q}_4}) - e(\tilde{S}^x_{\mathbf{q}-\mathbf{q}_0} - \tilde{S}^x_{\mathbf{q}+\mathbf{q}_0}) \\ b\tilde{S}^z_{\mathbf{q}} - d(\tilde{S}^z_{\mathbf{q}-2\mathbf{q}_4} + \tilde{S}^z_{\mathbf{q}+2\mathbf{q}_4}) + a\tilde{S}^x_{\mathbf{q}-\mathbf{q}_1} \\ - c(\tilde{S}^x_{\mathbf{q}-\mathbf{q}_0} + \tilde{S}^x_{\mathbf{q}+\mathbf{q}_0}) \\ + e(\tilde{S}^z_{\mathbf{q}-\mathbf{q}_0} - \tilde{S}^z_{\mathbf{q}+\mathbf{q}_0}) + f(\tilde{S}^x_{\mathbf{q}+2\mathbf{q}_4} - \tilde{S}^x_{\mathbf{q}-2\mathbf{q}_4}) \\ \tilde{S}^y_{\mathbf{q}} \end{pmatrix}, \tag{38}$$

where

$$a = \frac{1}{3}(\cos\alpha + \cos\beta + \cos\gamma),$$

$$b = \frac{1}{3}(\sin\alpha + \sin\beta + \sin\gamma),$$

$$c = \frac{1}{6}(\cos\beta + \cos\gamma - 2\cos\alpha),$$

$$d = \frac{1}{6}(\sin\beta + \sin\gamma - 2\sin\alpha),$$

$$e = \frac{i}{2\sqrt{3}}(\sin\beta - \sin\gamma),$$

$$f = \frac{i}{2\sqrt{3}}(\cos\beta - \cos\gamma) \tag{39}$$

are some abbreviations for the angular variables. For vanishing field Eqs. (39) reduce to

$$a = b = d = f = 0, \quad c = -\frac{1}{2}, \quad e = \frac{i}{2}, \tag{40}$$

i.e., the spin variables already given in Eq. (21).

Inserting Eq. (38) in the Hamiltonian of Eq. (26), truncating after the harmonic terms and diagonalizing the resulting

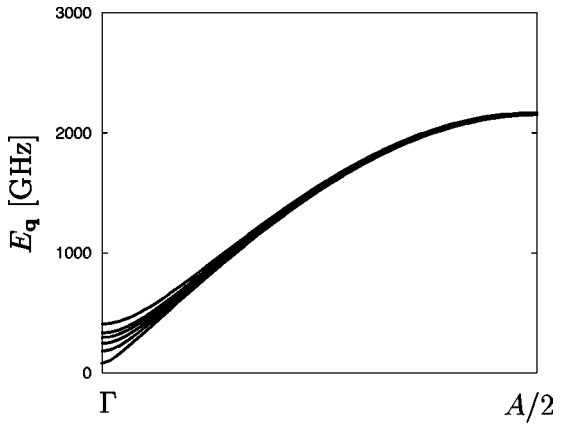

FIG. 17. Spin-wave frequencies in chain direction in the two-sublattice phase for $CsMnBr_3$ for a magnetic field $H_0=6.5$ T $>H_c$.

Hamiltonian leads to the spin-wave frequencies (see Fig. 17) (in Appendix A 2 we give the expressions for the two-sublattice case explicitly).

The dipolar energy leads to a lifting of the Goldstone mode present for the field-free case. This is in contrast to the spectrum obtained for a field applied *in* the chain direction, where a Goldstone mode still remains. Here the magnetic field forces the spins to align partially in field direction, whereas the dipolar energy fixes the spins within the basal planes; a free rotation of the ground-state configuration around the field direction is therefore impossible in contrast to a field applied in chain direction. This is the physical explanation for the gap in the excitation spectrum.

In the rest of the Brillouin zone the spectra for an applied field parallel and perpendicular to the chain direction are basically the same, i.e., the dipolar energy only changes the structure of the excitation spectra near the center of the Brillouin zone. However, we will see that these differences around $\mathbf{q}=0$ are crucial for the dependence of the magnetization on the field direction.

VI. FIELD DEPENDENT MAGNETIZATION AND COMPARISON WITH THE EXPERIMENT

We now turn to the field dependence of the magnetization of a dipolar, hexagonal antiferromagnet taking into account fluctuations. We will again distinguish between fields applied in the chain direction and fields applied within the basal plane.

A. Theory

The magnetization can be found from the free energy F via

$$\mathbf{M}=-\frac{\partial F}{\partial \mathbf{H}_0}. \tag{41}$$

The free energy is related to the partition function Z and the Hamiltonian H by

$$F=-kT\ \ln Z \quad \text{and} \quad Z=\mathrm{Sp}\exp(-\beta H), \tag{42}$$

where $\beta=1/k_BT$. For a field in the chain direction the Hamiltonian is given in Eq. (A1) and leads to

$$F_{\parallel}=E_g+\frac{1}{12}\sum_{\mathbf{q}}\ (E_{\mathbf{q}}^{(i)}-A_{\mathbf{q}}-A_{\mathbf{q}-\mathbf{q}_0}-A_{\mathbf{q}+\mathbf{q}_0}-A_{\mathbf{q}-2\mathbf{q}_0}$$
$$-A_{\mathbf{q}+2\mathbf{q}_0}-A_{\mathbf{q}-3\mathbf{q}_0})+k_BT\sum_{\mathbf{q}}\ \ln(1-e^{-\beta E_{\mathbf{q}}^{(i)}}), \tag{43}$$

where $\mathbf{q}$ runs over the magnetic Brillouin zone, $E_{\mathbf{q}}^{(i)}$ are the six branches of the magnon spectrum for the case of a field applied in chain direction, and $A_{\mathbf{q}}$ is given in Eq. (A2). For the Hamiltonian of Eq. (A3) (i.e., a field applied within the basal planes) one gets

$$F_{\perp}=E_g+\frac{1}{12}\sum_{\mathbf{q}}\ (E_{\mathbf{q}}^{(i)}-A_{\mathbf{q}}-A_{\mathbf{q}-\mathbf{q}_0}-A_{\mathbf{q}+\mathbf{q}_0}-A_{\mathbf{q}-2\mathbf{q}_4}$$
$$-A_{\mathbf{q}+2\mathbf{q}_4}-A_{\mathbf{q}-\mathbf{q}_1})+k_BT\sum_{\mathbf{q}}\ \ln(1-e^{-\beta E_{\mathbf{q}}^{(i)}}). \tag{44}$$

The $E_{\mathbf{q}}^{(i)}$ are again the six branches of the magnon spectrum, but now the ones gained for an applied field within the basal planes and $A_{\mathbf{q}}$ is given in Eq. (A5).

Generally, the free energy has three contributions: the first one is the classical ground-state energy, the second one is due to quantum fluctuations, whereas the third one is the contribution of thermal fluctuations. To calculate the free energy we replace the sums in Eqs. (43), (44) by integrals over the Brillouin zone. Then we have to integrate over the field-dependent spectra for different field strength. Differentiating these free energies with respect to the field leads to the magnetization. For the magnetization we find the same structure with classical, quantum, and thermal contributions.

The integration over the spectrum and the differentiation with respect to the applied field are done numerically. For the angles α,β, and γ, which cannot be given analytically, we use the numerically calculated values from the energy minimization of Eq. (31), see Fig. 15.

1. Classical contributions

The classical contributions to the magnetization are calculated via the classical ground-state energies. This yields

$$M_{\parallel}/Ng\mu_B=S\sin\varphi, \tag{45}$$

$$M_{\perp}/Ng\mu_B=\frac{1}{3}S(\sin\alpha+\sin\beta+\sin\gamma) \tag{46}$$

for the field parallel ($M_{\parallel}$) and perpendicular ($M_{\perp}$) to the chain direction, respectively. $M_{\parallel}$ can be calculated analytically [$\sin\varphi$ is given in Eq. (28)], whereas $M_{\perp}$ has to be calculated numerically as the equations following from Eq. (31) do not have analytic solutions for the tilting angles α,β,γ.

The classical results, which are plotted in Fig. 18, show not only an anisotropy for fields $H_0<H_c$, but also for fields $H_0>H_c$. The latter cannot be seen very clearly in Fig. 18 as the difference of the values of the magnetization for fields

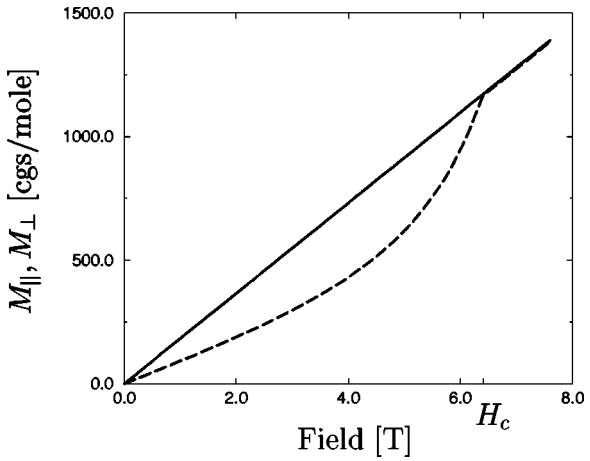

FIG. 18. Classical results for the magnetization for $CsMnBr_3$ ($J=213$ GHz, $J'=0.50$ GHz). Full line: field in chain direction, dashed line: field within the basal plane.

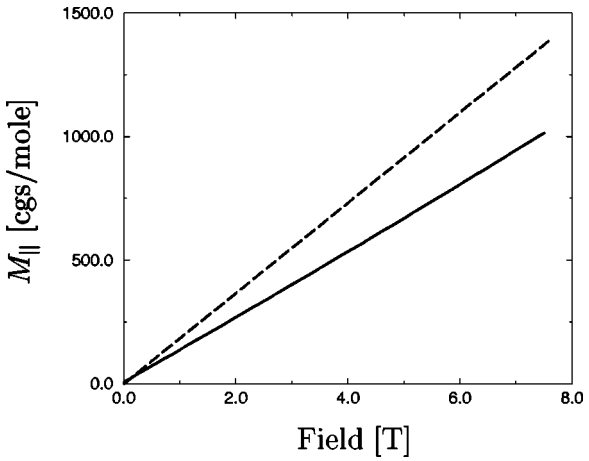

FIG. 19. Magnetization in $CsMnBr_3$. The full line is calculated under consideration of quantum fluctuations, the dashed line is the classical result.

$H_0 > H_c$ is proportional to the dipolar energy. However, the magnetization for fields parallel to the chain direction is always larger than for fields perpendicular to the chain direction, a fact that can also be seen in experiments.[27] This anisotropy is of dipolar origin since it is energetically more favorable for two spins to align ferromagnetically along their connecting line than perpendicular to it, which means in our case, that the spins can be tilted *in* the chain direction more easily. However, there are two discrepancies between the classical results and the measurements, namely, the absolute values are different and the experimental anisotropy found for $H_0 > H_c$ is much bigger than the one resulting from Eqs. (45), (46).[27] In the following we will show that mainly quantum fluctuations account for this large effect.

2. Quantum contributions

With the term quantum contributions we address the contributions also present at $T=0$, which are given by the derivative of the second term in Eqs. (43), (44). These contributions were evaluated numerically for the two field directions. One main result of these calculations is, that quantum fluctuations reduce the absolute value of the classical magnetization by up to 30%.

Field in chain direction. For a field in chain direction quantum fluctuations reduce the magnetization in the whole spin-flop phase. In Fig. 19 we plotted the magnetization for field strengths which can be reached in the experiment for the parameters of $CsMnBr_3$. The dashed line in Fig. 19 is equivalent to the full line in Fig. 18.

Field perpendicular to the chain direction. For fields within the basal plane we obtain the curves plotted in Fig. 20. Our method leads to an unphysical discontinuity of the magnetization at the transition from the three-sublattice to the two-sublattice phase. Moreover, at the phase transition to the paramagnetic phase we not only find a discontinuity in the magnetization but we also get absolute values of the magnetization which are larger than the saturation magnetization. Exactly the same results were theoretically found by Rastelli *et al.*[28] for the case of ferromagnetic spin chains which are coupled antiferromagnetically on a hexagonal lattice. These authors claim, that the discontinuities show, that the system is in some kind of intermediate phase in the transition regions, which consists of a mixture of the two adjacent phases. Therefore they perform a Maxwell construction in the free energy and get a plateau in the magnetization.[28]

However, there is no significance for such a plateau in any of the experiments on hexagonal antiferromagnets.[27,29] Moreover, the motivation to perform a Maxwell construction in the free energy in the regions of the phase transitions is not obvious to us. In Sec. VI B we will show that the method of calculating the magnetization as the derivative of the free energy seems questionable at phase transitions.

3. Thermal fluctuations

Let us now discuss the influence of the third term in Eqs. (43), (44). These terms lead to contributions to the free energy due to thermal fluctuations ($T>0$). To estimate the effect of thermal fluctuations one would have to compare the temperature at which the measurements were made with the

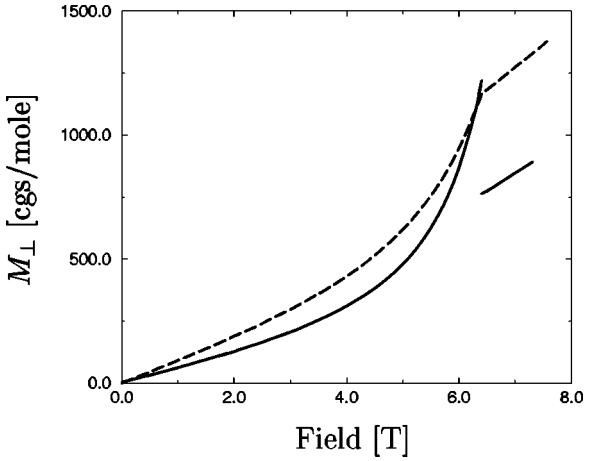

FIG. 20. Magnetization in $CsMnBr_3$. The full line is under consideration of quantum fluctuations, the dashed line is the classical result.

one corresponding to the anisotropy. However, we performed a numerical calculation of the integrals, which shows that thermal contributions are not important at temperatures at which the experiments are performed. For $CsMnBr_3$, which has a Neél temperature of $T_N=8.3$ K,[23] one gets for $T=1.8$ K, a typical temperature where measurements in the ordered phase are performed

$$F_{\rm th}(T=1.8\ \ {\rm K})/F_0 \lesssim 10^{-4}.$$

Thermal fluctuations therefore cannot be responsible for the large anisotropies in the field-dependent magnetization, compare Ref. 30.

B. Results for a topological similar dipolar system

For hexagonal antiferromagnets without dipolar energy it was shown by Zhitomirsky and Zaliznyak[31] that the magnetization is different depending on whether one calculates the derivative of the free energy or the mean value of the spin projection on the magnetic field. However, these authors were able to show, that the two results are the same up to the first order in the ratio J'/J in these systems. Santini *et al.*[14] also called attention to this fact. However, they analyzed the magnetization by means of a Monte Carlo simulation.

In the following we study the phase diagram and the resulting magnetization for the two-dimensional dipolar antiferromagnet on a square lattice with longitudinal field. The reason to investigate this system is that its phase diagram has the same topology as the one of the hexagonal antiferromagnet, i.e., it has phases which can, depending on the magnitude of the field, classically be described by one or two independent angles with respect to the applied field. The phase which is parametrized by two angles is called the intermediate phase, whereas the phase where one angle suffices is the spin-flop phase.[32] At a critical field strength the system undergoes the same kind of phase transition as the hexagonal antiferromagnet, namely two angles coincide. For high fields we find a transition to a paramagnetic phase in both systems.

However, in the two-dimensional system we are able to calculate the magnetization not only by using the free energy but also by directly calculating the mean value of the spin projection on the field. In principle, this is also possible for the dipolar, hexagonal antiferromagnet, but fails due to the complicated Hamiltonian of Eq. (A3). Due to the six sublattices one would have to calculate six Greens functions out of the twelve equations of motions (i.e., the *eigenvectors* of the equations of motion) and integrate them over the first BZ, which is a numerically hopeless task. Note that we only had to calculate the *eigenvalues* of the matrix describing the equation of motion to find the magnon energies $E_{\mathbf{q}}^{(i)}$, which are needed to calculate the free energy. All in all this means that we are numerically able to calculate the free energy, whereas the direct calculation of the magnetization is numerically not feasible in the case of the dipolar, hexagonal antiferromagnet.

Let us now return to the magnetization in the two-dimensional dipolar antiferromagnet. First of all we note that the classical magnetization curve was studied by one of the authors (compare Ref. 32). In the following we are interested in the behavior of the magnetization *including* fluctuations. In particular, we study the magnetization at the phase transition from the intermediate to the spin-flop phase and at higher fields from the spin-flop phase to the paramagnetic phase.

As already stressed, we will calculate the magnetization not only via the free energy but also via the mean value of the spin on the field direction. This can be done using the Greens function technique.[21] The magnetization in the spin-flop phase is, for instance, given by

$$M=g\mu_B\sum\ \langle S_l^z\rangle$$

$$=Ng\mu_B S\sin\gamma\left(1-\frac{1}{S}\sum_{\mathbf{q}}\ \langle a_{\mathbf{q}}^\dagger a_{\mathbf{q}}\rangle\right), \qquad (47)$$

where γ is the classical tilt angle of the spins with respect to the magnetic field and the z direction is the field direction. The mean value $\langle a_{\mathbf{q}}^\dagger a_{\mathbf{q}}\rangle$ is calculated via the spectral theorem

$$\langle a_{\mathbf{q}}^\dagger a_{\mathbf{q}}\rangle=\frac{i}{2\pi}\int d\omega[G_1(\omega+i\delta)-G_1(\omega-i\delta)]n(\omega), \qquad (48)$$

where $G_1=\langle\langle a_{\mathbf{q}};a_{\mathbf{q}}^\dagger\rangle\rangle$ is given as the eigenvector of the equations of motions for G_1 and three other Greens functions and can be calculated straight forward. $\mathbf{q}_0=(\pi/a)(1,1)$ mediates between the two sublattices of the system. To get the magnetization one has to evaluate an integration over a Greens function in Eq. (47). We stress again that in principle the same proceeding is possible in the hexagonal antiferromagnet; however, in those systems the three-dimensional integrals can no longer be evaluated numerically with sensible accuracy due to computational time problems, as one has twelve equations of motions and therefore very complicated integrals.

The free energy for the two-dimensional antiferromagnet is given by

$$F=E_g-\frac{1}{4}\sum_{\rm cryst\ BZ}(A_{\mathbf{q}}+A_{\mathbf{q}+\mathbf{q}_0}-E_{\mathbf{q}}^{(1)}-E_{\mathbf{q}}^{(2)}), \qquad (49)$$

where E_g is the classical ground state energy, $E_{\mathbf{q}}^{(1)}$,$E_{\mathbf{q}}^{(2)}$ are the magnon energies of the two branches, and $A_{\mathbf{q}}$ is the coefficient of the diagonal term in the Hamiltonian before the diagonalization.

Numerical results. In Fig. 21 we plotted numerical results of the magnetization. The evaluation of the magnetization using the derivative of the free energy leads to discontinuities at all phase transitions. At the phase transition from the spin-flop to the paramagnetic phase (Fig. 21) the magnetization for fields lower than the transition field is again larger than the saturation magnetization. These results are qualitatively the same as the ones found in the previous section for hexagonal antiferromagnets and the ones found by Rastelli *et al.*[28]

However, here we calculated the magnetization also as the mean value of the spin projection on the field (full line in Fig. 21); in this calculation one does not get a discontinuity

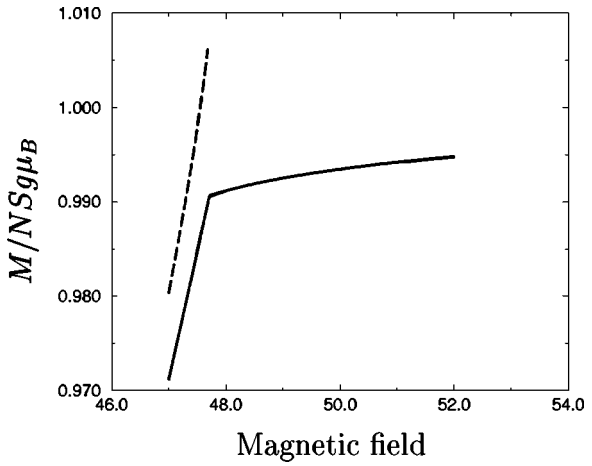

FIG. 21. Magnetization at the phase transition from the spin flop to the paramagnetic phase. Dashed line: results from the free energy, full line: results from the spectral theorem. In the paramagnetic phase one gets identical curves. The magnetic field is given in units of $g\mu_B$.

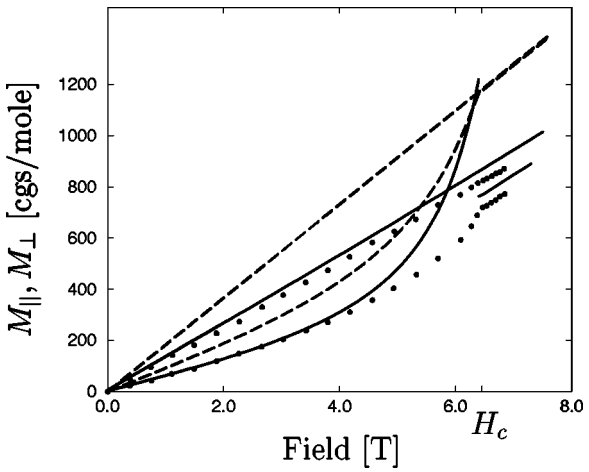

FIG. 22. Longitudinal and transverse magnetization for $CsMnBr_3$ compared with the experiment (Ref. 27). Dashed: classical theory, solid: quantum mechanical theory with fluctuations, points: experiment. The upper curves belong to a field in chain direction, the lower ones to a field perpendicular to the chain direction.

in the magnetization. Moreover, also the absolute value of the magnetization is always lower than the saturation magnetization. The calculation using the spectral theorem therefore seems to give more reasonable results than the one using the free energy. However, for decreasing fields in the spin-flop phase, the two curves in Fig. 21 converge. This qualitative behavior is again gained at all phase transitions.

Our conclusion from all that is that the magnetization calculated using the free energy is not a good approximation at phase transitions but approaches the more reasonable results calculated by means of the spectral theorem for fields that are not too close to phase transitions. Comparing Eqs. (47) and (49) shows again that the calculation of the magnetization via the free energy just requires us to evaluate *eigenvalues* of the equations of motions, whereas calculating the magnetization using Eq. (47) requires us to determine the *eigenvectors*, namely, the full Greens functions of the system and is therefore much more complicated. However, the latter calculation also yields meaningful results at phase transitions whereas the first one fails in these regions.

C. Comparison with experiment

In Fig. 22 we have plotted the results from Sec. VI B and the experimental data on $CsMnBr_3$.[27] Note that no additional free parameter enters in the results of Fig. 22 as the dipolar anisotropy is fixed by the magnetic moment and the lattice structure. The intrachain-interaction J is determined by comparing dispersion relations with measurements of magnons along the chain direction in the one-dimensional short-range regime.[33] The advantage of this method is that for temperatures above the three-dimensional ordering temperature $T > T_N$ the intrachain-interaction is the only relevant interaction and can therefore be fixed accurately. The interchain-interaction J' can be determined by comparing spin waves in the three-dimensionally ordered phase measured perpendicular to the chain axis with theoretical results. However, one gets different parameters in dependence on the kind of spin models one uses. Therefore, we determine J' out of the critical field in Eq. (33). In this case the critical field is to lowest order independent on the additional kind of anisotropy in the Heisenberg model.

In this paper we have made use of the parameter set

$$J = 213 \text{ GHz} = 0.88 \text{ meV} = 10.21 \text{ K}, \quad J' = 0.50 \text{ GHz} \tag{50}$$

which leads to a critical field of $H_c = 6.4$ T.

In Fig. 22 one sees that we get good agreement of our theory with the experiment for a field applied in the chain direction. The absolute value of the magnetization is a bit too large. We will come to that point later on. For a field applied perpendicular to the chain direction we find good agreement for low fields whereas the influence of fluctuations at the phase transition is underestimated. The curve which is calculated under consideration of fluctuations converges to the classical one at $H \approx H_c$. In the previous section we have shown that the results for the magnetization calculated using the free energy are questionable near phase transitions.

However, for fields $H > H_c$ we get very good agreement for the *ratio* of the magnetization for a field in chain direction to the magnetization for a field within the basal plane. As this ratio is almost independent of the exact parameter set one uses for the exchange interaction we conclude that this result shows the effect of fluctuations in the *dipolar* Hamiltonian. The dipolar interaction therefore is not only responsible for the kind of anisotropies in all ground states but also gives rise to the anisotropy in the field-dependent magnetization. This reflects the fact that the dispersion relations are qualitatively different for the two field directions if one considers the additional dipolar interaction in the exchange Hamiltonian of Eq. (1). One finds a remaining Goldstone mode for a field in the chain direction whereas no Goldstone mode is present for fields applied within the basal plane (see Secs. V A, and V B).

The occurrence of a large anisotropy in the magnetization for fields $H>H_c$ can even be explained in a pure one-dimensional model,[36] but without qualitative agreement. The absolute values of the magnetizations are too large compared to experiments. This is in part due to a certain experimental uncertainty as the measurements have to be calibrated when measuring absolute values. Therefore different experimental groups get slightly different absolute values for the magnetizations, but almost identical values for the anisotropy of the magnetization for $H>H_c$.[27,34,35] On the other hand, one gets virtually the exact agreement of the magnetization for $H>H_c$ if one uses a slightly larger value for the intrachain interaction, namely, $J=222$ GHz. This is a difference in the intrachain interaction of 4% to the value we used for the calculations [Eq. (50)] and which was gained by a pure one-dimensional model.

VII. SUMMARY

We investigated a dipolar Heisenberg model as a model for hexagonal antiferromagnets. We found three commensurate and two incommensurate phases for different values of the ratio of dipolar to interchain interaction in the field free case. We showed via linear spin-wave theory that all of these commensurate phases are stable against fluctuations and that the incommensurate phase IC II can be approximated by a 120° structure for weak dipolar energies.

The spin-wave frequencies of our theoretical model are in good agreement with neutron scattering experiments on $CsMnBr_3$ and $RbMnBr_3$, which shows that the dipolar energy is the most important source of anisotropy in these Mn compounds.

The ground states for fields along and perpendicular to the chain direction were studied for low dipolar energies. For a field along the chain axis it turns out that an umbrella phase is the ground-state configuration for nonvanishing fields; for high fields a paramagnetic phase is established. Applying a field within the basal plane shows the following. First, the dipolar energy leading to an in-plane anisotropy in the field-free case is strong enough to keep the spins within the basal plane for all field strengths. Secondly, a three-sublattice ground state configuration is established for low field strength. Two out of the three angles coincide as the field reaches a critical field H_c and the reorientation of the spins appears in the same way as in an ordinary two-sublattice spin-flop phase despite the fact that the two remaining spins enclose slightly different angles with the field direction.

Based on these ground states we performed a spin-wave calculation by means of a Holstein-Primakoff transformation. We calculated the magnons in all of the above mentioned phases; we found qualitatively different magnon spectra for the same field strength depending on the direction of the applied field. Whereas the excitation spectrum for the umbrella phase is gapless, the excitation spectrum for the three- and two-sublattice phase is gaped. This is due to the different symmetry of the ground states.

The field-dependent magnetization including fluctuations was studied in a next step and we compared our findings with experiments. Calculating the magnetization via the free energy leads to unphysical discontinuities for fields applied within the basal plane at the phase transitions from the three sublattice to the two sublattice and from the two sublattice to the paramagnetic phase. Studying a system where one can calculate the magnetization not only via the free energy but also via the mean value of the spin projection shows that the results obtained by using the free energy are questionable at phase transitions, but converge to the results using the mean value away from phase transitions. We found that the big anisotropy in the magnetization for a field parallel and perpendicular to the chain direction present for high fields is due to quantum fluctuations rather than thermal fluctuations and found excellent agreement between our dipolar theory and the experiment.

ACKNOWLEDGMENTS

This work was supported by the BMBF under Contract No. 03-SC5-TUM 0 and the DFG under Contract No. Schw 348/10-1.

APPENDIX A: SIX-SUBLATTICE CONFIGURATION

In the body of the paper we displayed our results by plotting spin-wave spectra for different phases, see Figs. 12, 17. In this appendix we give the longish formulas for the calculation of these spin-waves in the harmonic approximation.

1. Field along the chain direction

For a field along the chain direction the ground state is an umbrella phase as shown in Sec. V A. The transformation for the spin components is given Eq. (21). After inserting this transformation in Eq. (26) and truncating after the harmonic terms, the Hamiltonian reads

$$
\begin{aligned}
H=E_g+\sum_{\mathbf{q}}\Big\{&A_{\mathbf{q}}a^{\dagger}_{\mathbf{q}}a_{\mathbf{q}}+\frac{1}{2}B_{\mathbf{q}}a_{\mathbf{q}}a_{-\mathbf{q}}+\frac{1}{2}B^{*}_{\mathbf{q}}a^{\dagger}_{\mathbf{q}}a^{\dagger}_{-\mathbf{q}}+C_{\mathbf{q}}a_{\mathbf{q}}a_{-\mathbf{q}+2\mathbf{q}_0}+C^{*}_{\mathbf{q}}a^{\dagger}_{\mathbf{q}}a^{\dagger}_{-\mathbf{q}+2\mathbf{q}_0}+D_{\mathbf{q}}a_{\mathbf{q}}a_{-\mathbf{q}-2\mathbf{q}_0}+D^{*}_{\mathbf{q}}a^{\dagger}_{\mathbf{q}}a^{\dagger}_{-\mathbf{q}-2\mathbf{q}_0}\\
&+E_{\mathbf{q}}a^{\dagger}_{\mathbf{q}}a_{\mathbf{q}+2\mathbf{q}_0}+E^{*}_{\mathbf{q}}a^{\dagger}_{\mathbf{q}+2\mathbf{q}_0}a_{\mathbf{q}}+F_{\mathbf{q}}a^{\dagger}_{\mathbf{q}}a_{\mathbf{q}-2\mathbf{q}_0}+F^{*}_{\mathbf{q}}a^{\dagger}_{\mathbf{q}-2\mathbf{q}_0}a_{\mathbf{q}}+G_{\mathbf{q}}a_{\mathbf{q}}a_{-\mathbf{q}+\mathbf{q}_0}+G^{*}_{\mathbf{q}}a^{\dagger}_{\mathbf{q}}a^{\dagger}_{-\mathbf{q}+\mathbf{q}_0}+H_{\mathbf{q}}a_{\mathbf{q}}a_{-\mathbf{q}-\mathbf{q}_0}\\
&+H^{*}_{\mathbf{q}}a^{\dagger}_{\mathbf{q}}a^{\dagger}_{-\mathbf{q}-\mathbf{q}_0}+I_{\mathbf{q}}a^{\dagger}_{\mathbf{q}}a_{\mathbf{q}+\mathbf{q}_0}+I^{*}_{\mathbf{q}}a^{\dagger}_{\mathbf{q}+\mathbf{q}_0}a_{\mathbf{q}}+J_{\mathbf{q}}a^{\dagger}_{\mathbf{q}}a_{\mathbf{q}-\mathbf{q}_0}+J^{*}_{\mathbf{q}}a^{\dagger}_{\mathbf{q}-\mathbf{q}_0}a_{\mathbf{q}}\Big\}. \qquad \text{(A1)}
\end{aligned}
$$

The ground-state energy is given in Eq. (27). The coefficients in the Hamiltonian (A1) are given by

$$A_{\mathbf{q}}=2S(J_{\mathbf{q}_0}+A^{11}_{\mathbf{q}_0})-S\cos^2\varphi(J_{\mathbf{q}}+A^{33}_{\mathbf{q}})-\frac{1}{4}S\sin^2\varphi(2J_{\mathbf{q}+\mathbf{q}_0}+2J_{\mathbf{q}-\mathbf{q}_0}+A^{11}_{\mathbf{q}+\mathbf{q}_0}+A^{11}_{\mathbf{q}-\mathbf{q}_0}+A^{22}_{\mathbf{q}+\mathbf{q}_0}+A^{22}_{\mathbf{q}-\mathbf{q}_0})$$
$$-\frac{1}{4}S\sin\varphi(2J_{\mathbf{q}+\mathbf{q}_0}-2J_{\mathbf{q}-\mathbf{q}_0}+A^{11}_{\mathbf{q}+\mathbf{q}_0}-A^{11}_{\mathbf{q}-\mathbf{q}_0}+A^{22}_{\mathbf{q}+\mathbf{q}_0}-A^{22}_{\mathbf{q}-\mathbf{q}_0})-\frac{1}{4}S(2J_{\mathbf{q}+\mathbf{q}_0}+2J_{\mathbf{q}-\mathbf{q}_0}$$
$$+A^{11}_{\mathbf{q}+\mathbf{q}_0}+A^{11}_{\mathbf{q}-\mathbf{q}_0}+A^{22}_{\mathbf{q}+\mathbf{q}_0}+A^{22}_{\mathbf{q}-\mathbf{q}_0}),$$

$$B_{\mathbf{q}}=\frac{1}{4}S\sin^2\varphi(2J_{\mathbf{q}+\mathbf{q}_0}+2J_{\mathbf{q}-\mathbf{q}_0}+A^{11}_{\mathbf{q}+\mathbf{q}_0}+A^{11}_{\mathbf{q}-\mathbf{q}_0}+A^{22}_{\mathbf{q}+\mathbf{q}_0}+A^{22}_{\mathbf{q}-\mathbf{q}_0})-\frac{1}{4}S(2J_{\mathbf{q}+\mathbf{q}_0}+2J_{\mathbf{q}-\mathbf{q}_0}+A^{11}_{\mathbf{q}+\mathbf{q}_0}+A^{11}_{\mathbf{q}-\mathbf{q}_0}+A^{22}_{\mathbf{q}+\mathbf{q}_0}+A^{22}_{\mathbf{q}-\mathbf{q}_0})$$
$$+S\cos^2\varphi(J_{\mathbf{q}}+A^{33}_{\mathbf{q}})-i\frac{S}{2}\sin^2\varphi(A^{12}_{\mathbf{q}-\mathbf{q}_0}-A^{12}_{\mathbf{q}+\mathbf{q}_0})+i\frac{S}{2}(A^{12}_{\mathbf{q}-\mathbf{q}_0}-A^{12}_{\mathbf{q}+\mathbf{q}_0}),$$

$$C_{\mathbf{q}}=\frac{S}{8}\sin^2\varphi(A^{11}_{\mathbf{q}-\mathbf{q}_0}-A^{22}_{\mathbf{q}-\mathbf{q}_0})-\frac{S}{4}\sin\varphi(A^{11}_{\mathbf{q}-\mathbf{q}_0}-A^{22}_{\mathbf{q}-\mathbf{q}_0})+\frac{S}{8}(A^{11}_{\mathbf{q}-\mathbf{q}_0}-A^{22}_{\mathbf{q}-\mathbf{q}_0})+\frac{1}{4}iS\sin^2\varphi A^{12}_{\mathbf{q}-\mathbf{q}_0}-\frac{1}{2}iS\sin\varphi A^{12}_{\mathbf{q}-\mathbf{q}_0}+\frac{1}{4}iSA^{12}_{\mathbf{q}-\mathbf{q}_0}$$

$$D_{\mathbf{q}}=\frac{S}{8}\sin^2\varphi(A^{11}_{\mathbf{q}+\mathbf{q}_0}-A^{22}_{\mathbf{q}+\mathbf{q}_0})-\frac{S}{4}\sin\varphi(A^{11}_{\mathbf{q}+\mathbf{q}_0}-A^{22}_{\mathbf{q}+\mathbf{q}_0})+\frac{S}{8}(A^{11}_{\mathbf{q}+\mathbf{q}_0}-A^{22}_{\mathbf{q}+\mathbf{q}_0})$$
$$+\frac{1}{4}iS\sin^2\varphi A^{12}_{\mathbf{q}+\mathbf{q}_0}-\frac{1}{2}iS\sin\varphi A^{12}_{\mathbf{q}+\mathbf{q}_0}-\frac{1}{4}iSA^{12}_{\mathbf{q}+\mathbf{q}_0},$$

$$E_{\mathbf{q}}=-\frac{S}{8}\sin^2\varphi(A^{11}_{\mathbf{q}+\mathbf{q}_0}-A^{22}_{\mathbf{q}+\mathbf{q}_0})+\frac{S}{8}(A^{11}_{\mathbf{q}+\mathbf{q}_0}-A^{22}_{\mathbf{q}+\mathbf{q}_0})+\frac{1}{4}iS\sin^2\varphi A^{12}_{\mathbf{q}+\mathbf{q}_0}+\frac{1}{4}iSA^{12}_{\mathbf{q}+\mathbf{q}_0},$$

$$F_{\mathbf{q}}=-\frac{S}{8}\sin^2\varphi(A^{11}_{\mathbf{q}-\mathbf{q}_0}-A^{22}_{\mathbf{q}-\mathbf{q}_0})+\frac{S}{8}(A^{11}_{\mathbf{q}-\mathbf{q}_0}-A^{22}_{\mathbf{q}-\mathbf{q}_0})-\frac{1}{4}iS\sin^2\varphi A^{12}_{\mathbf{q}+\mathbf{q}_0}-\frac{1}{4}iSA^{12}_{\mathbf{q}+\mathbf{q}_0},\tag{A2}$$

$$G_{\mathbf{q}}=-\frac{S}{2}\sin\varphi\ \cos\varphi A^{13}_{\mathbf{q}-\mathbf{q}_0}+\frac{S}{2}\cos\varphi A^{13}_{\mathbf{q}-\mathbf{q}_0}-i\frac{S}{2}\sin\varphi\cos\varphi A^{23}_{\mathbf{q}-\mathbf{q}_0}+i\frac{S}{2}\cos\varphi A^{23}_{\mathbf{q}-\mathbf{q}_0},$$

$$H_{\mathbf{q}}=-\frac{S}{2}\sin\varphi\cos\varphi A^{13}_{\mathbf{q}+\mathbf{q}_0}-\frac{S}{2}\cos\varphi A^{13}_{\mathbf{q}+\mathbf{q}_0}+i\frac{S}{2}\sin\varphi\cos\varphi A^{23}_{\mathbf{q}+\mathbf{q}_0}+i\frac{S}{2}\cos\varphi A^{23}_{\mathbf{q}+\mathbf{q}_0}$$

$$I_{\mathbf{q}}=\frac{S}{2}\sin\varphi\cos\varphi A^{13}_{\mathbf{q}+\mathbf{q}_0}+\frac{S}{2}\cos\varphi A^{13}_{\mathbf{q}+\mathbf{q}_0}+i\frac{S}{2}\sin\varphi\cos\varphi A^{23}_{\mathbf{q}+\mathbf{q}_0}+i\frac{S}{2}\cos\varphi A^{23}_{\mathbf{q}+\mathbf{q}_0},$$

$$J_{\mathbf{q}}=\frac{S}{2}\sin\varphi\cos\varphi A^{13}_{\mathbf{q}-\mathbf{q}_0}-\frac{S}{2}\cos\varphi A^{13}_{\mathbf{q}-\mathbf{q}_0}-i\frac{S}{2}\sin\varphi\cos\varphi A^{23}_{\mathbf{q}-\mathbf{q}_0}+i\frac{S}{2}\cos\varphi A^{23}_{\mathbf{q}-\mathbf{q}_0},$$

where $\sin\varphi$ is given in Eq. (28). The case of vanishing field is contained in these formulas for $\varphi=0$.

2. Field perpendicular to the chain direction

To calculate the magnon spectrum for a field applied within basal lattice planes, we have to insert Eq. (38) into the Hamiltonian of Eq. (26). In the following we give the expressions for fields $H>H_c$ explicitly, where the ground state can be parametrized by two angles α and $\beta=\gamma$. This implies $e=f=0$ in Eq. (39). For the general case of three sublattices the formulas are more complicated. The quadratic Hamiltonian reads

$$H=E_g+\sum_{\mathbf{q}} A_{\mathbf{q}}a^{\dagger}_{\mathbf{q}}a_{\mathbf{q}}+\frac{1}{2}B_{\mathbf{q}}a_{\mathbf{q}}a_{-\mathbf{q}}+\frac{1}{2}B^{*}_{\mathbf{q}}a^{\dagger}_{\mathbf{q}}a^{\dagger}_{-\mathbf{q}}+C_{\mathbf{q}}a_{\mathbf{q}}a_{-\mathbf{q}+2\mathbf{q}_4}+C^{*}_{\mathbf{q}}a^{\dagger}_{\mathbf{q}}a^{\dagger}_{-\mathbf{q}+2\mathbf{q}_4}+D_{\mathbf{q}}a^{\dagger}_{\mathbf{q}}a_{\mathbf{q}-2\mathbf{q}_4}+D^{*}_{\mathbf{q}}a_{\mathbf{q}}a^{\dagger}_{\mathbf{q}-2\mathbf{q}_4}+E_{\mathbf{q}}a_{\mathbf{q}}a_{-\mathbf{q}-2\mathbf{q}_4}$$

$$+E^{*}_{\mathbf{q}}a^{\dagger}_{\mathbf{q}}a^{\dagger}_{-\mathbf{q}-2\mathbf{q}_4}+F_{\mathbf{q}}a^{\dagger}_{\mathbf{q}}a_{\mathbf{q}+2\mathbf{q}_4}+F^{*}_{\mathbf{q}}a_{\mathbf{q}}a^{\dagger}_{\mathbf{q}+2\mathbf{q}_4}+G_{\mathbf{q}}(a^{\dagger}_{\mathbf{q}}a_{\mathbf{q}+\mathbf{q}_1}+a_{\mathbf{q}}a_{-\mathbf{q}-\mathbf{q}_1})+G^{*}_{\mathbf{q}}(a_{\mathbf{q}}a^{\dagger}_{\mathbf{q}+\mathbf{q}_1}+a^{\dagger}_{\mathbf{q}}a^{\dagger}_{-\mathbf{q}-\mathbf{q}_1})$$

$$+H_{\mathbf{q}}(a^{\dagger}_{\mathbf{q}}a_{\mathbf{q}+\mathbf{q}_0}+a_{\mathbf{q}}a_{-\mathbf{q}-\mathbf{q}_0})+H^{*}_{\mathbf{q}}(a_{\mathbf{q}}a^{\dagger}_{\mathbf{q}+\mathbf{q}_0}+a^{\dagger}_{\mathbf{q}}a^{\dagger}_{-\mathbf{q}-\mathbf{q}_0})+I_{\mathbf{q}}(a^{\dagger}_{\mathbf{q}}a_{\mathbf{q}-\mathbf{q}_0}+a_{\mathbf{q}}a_{-\mathbf{q}+\mathbf{q}_0})+I^{*}_{\mathbf{q}}(a_{\mathbf{q}}a^{\dagger}_{\mathbf{q}-\mathbf{q}_0}+a^{\dagger}_{\mathbf{q}}a^{\dagger}_{-\mathbf{q}+\mathbf{q}_0}). \tag{A3}$$

The ground state energy in the crystallographic Brillouin zone which is equivalent to formula (31) (where the energy is given in the magnetic Brillouin zone) reads

$$E_g=-NS^2[a^2(J_{\mathbf{q}_1}+A^{11}_{\mathbf{q}_1})+2c^2(J_{\mathbf{q}_0}+A^{11}_{\mathbf{q}_0})-2f^2(J_{2\mathbf{q}_4}+A^{11}_{2\mathbf{q}_4})+b^2(J_0+A^{22}_0)+2d^2(J_{2\mathbf{q}_4}+A^{22}_{2\mathbf{q}_4})-2e^2(J_{\mathbf{q}_0}+A^{22}_{\mathbf{q}_0})]-hNSb, \tag{A4}$$

with $h=g\mu_B H_0$. The coefficients in Eq. (A3) are given by

$$A_{\mathbf{q}}/S=\{[2(J_0+A^{22}_0)-(J_{\mathbf{q}}+A^{11}_{\mathbf{q}})]b^2+[2(J_{\mathbf{q}_1}+A^{11}_{\mathbf{q}_1})-(J_{\mathbf{q}+\mathbf{q}_1}+A^{22}_{\mathbf{q}+\mathbf{q}_1})]a^2$$
$$+[4(J_{\mathbf{q}_0}+A^{11}_{\mathbf{q}_0})-(J_{\mathbf{q}+\mathbf{q}_0}+J_{\mathbf{q}-\mathbf{q}_0}+A^{22}_{\mathbf{q}+\mathbf{q}_0}+A^{22}_{\mathbf{q}-\mathbf{q}_0})]c^2+[4(J_{2\mathbf{q}_4}+A^{22}_{2\mathbf{q}_4})-(J_{\mathbf{q}+2\mathbf{q}_4}+J_{\mathbf{q}-2\mathbf{q}_4}+A^{11}_{\mathbf{q}+2\mathbf{q}_4}+A^{11}_{\mathbf{q}-2\mathbf{q}_4})d^2]\}$$
$$-(J_{\mathbf{q}}+A^{33}_{\mathbf{q}})+g\mu_B H_0/Sb,$$

$$B_{\mathbf{q}}/S=-\{(J_{\mathbf{q}}+A^{11}_{\mathbf{q}})b^2+(J_{\mathbf{q}+\mathbf{q}_1}+A^{22}_{\mathbf{q}+\mathbf{q}_1})a^2+(J_{\mathbf{q}+\mathbf{q}_0}+J_{\mathbf{q}-\mathbf{q}_0}+A^{22}_{\mathbf{q}+\mathbf{q}_0}+A^{22}_{\mathbf{q}-\mathbf{q}_0})c^2+(J_{\mathbf{q}+2\mathbf{q}_4}+J_{\mathbf{q}-2\mathbf{q}_4}+A^{11}_{\mathbf{q}+2\mathbf{q}_4}+A^{11}_{\mathbf{q}-2\mathbf{q}_4})d^2\}$$
$$+(J_{\mathbf{q}}+A^{33}_{\mathbf{q}})-2iA^{13}_{\mathbf{q}}b,$$

$$C_{\mathbf{q}}/S=\frac{1}{2}\{(J_{\mathbf{q}}+A^{11}_{\mathbf{q}}+J_{\mathbf{q}-2\mathbf{q}_4}+A^{11}_{\mathbf{q}-2\mathbf{q}_4})bd+(J_{\mathbf{q}+\mathbf{q}_0}+A^{22}_{\mathbf{q}+\mathbf{q}_0}+J_{\mathbf{q}+\mathbf{q}_1}+A^{22}_{\mathbf{q}+\mathbf{q}_1})ac-(J_{\mathbf{q}+2\mathbf{q}_4}+A^{11}_{\mathbf{q}+2\mathbf{q}_4})d^2-(J_{\mathbf{q}-\mathbf{q}_0}+A^{22}_{\mathbf{q}-\mathbf{q}_0})c^2\}$$
$$+iA^{13}_{\mathbf{q}-2\mathbf{q}_4}d,$$

$$D_{\mathbf{q}}/S=\frac{1}{2}\{[-2(J_0+A^{22}_0+J_{2\mathbf{q}_4}+A^{22}_{2\mathbf{q}_4})+(J_{\mathbf{q}}+A^{11}_{\mathbf{q}}+J_{\mathbf{q}-2\mathbf{q}_4}+A^{11}_{\mathbf{q}-2\mathbf{q}_4})]bd$$
$$+[-2(J_{\mathbf{q}_1}+A^{11}_{\mathbf{q}_1}+J_{\mathbf{q}_0}+A^{11}_{\mathbf{q}_0})+(J_{\mathbf{q}+\mathbf{q}_0}+A^{22}_{\mathbf{q}+\mathbf{q}_0}+J_{\mathbf{q}+\mathbf{q}_1}+A^{22}_{\mathbf{q}+\mathbf{q}_1})]ac$$
$$+[2(J_{\mathbf{q}_0}+A^{11}_{\mathbf{q}_0})-(J_{\mathbf{q}-\mathbf{q}_0}+A^{22}_{\mathbf{q}-\mathbf{q}_0})]c^2+(2(J_{2\mathbf{q}_4}+A^{22}_{2\mathbf{q}_4})-(J_{\mathbf{q}+2\mathbf{q}_4}+A^{11}_{\mathbf{q}+2\mathbf{q}_4})]d^2\}+iA^{13}_{\mathbf{q}-2\mathbf{q}_4}d-\frac{1}{2}g\mu_B H_0/Sd,$$

$$E_{\mathbf{q}}=C_{-\mathbf{q}},$$

$$F_{\mathbf{q}}=D_{-\mathbf{q}},$$

$$G_{\mathbf{q}}/S=A^{12}_{\mathbf{q}}ab+(A^{12}_{\mathbf{q}+2\mathbf{q}_4}+A^{12}_{\mathbf{q}-2\mathbf{q}_4})cd+iA^{23}_{\mathbf{q}+\mathbf{q}_1}a,$$

$$H_{\mathbf{q}}/S=-A^{12}_{\mathbf{q}}bc+A^{12}_{\mathbf{q}+2\mathbf{q}_4}cd-A^{12}_{\mathbf{q}-2\mathbf{q}_4}ad-iA^{23}_{\mathbf{q}+\mathbf{q}_0}c,$$

$$I_{\mathbf{q}}=H_{-\mathbf{q}}. \tag{A5}$$

Here we used the abbreviations defined in Eqs. (39). The diagonalization of the Hamiltonians (A1), (A3) can be performed in an analogous way: the equation of motion for the Greens function $\langle\langle a_{\mathbf{q}};a^{\dagger}_{\mathbf{q}}\rangle\rangle$ with the Hamiltonians generate eleven other Greens functions leading to a system of twelve equations for the twelve Greens functions. The spin-wave frequencies are given by the eigenvalues of the resulting 12×12 matrix.

APPENDIX B: DIPOLAR ENERGY

In the body of the paper we gave formulas which contained Fourier transforms of the dipolar tensor. We have to distinguish between dipolar tensors in the crystallographic BZ and in the magnetic BZ. The formulas for the dipolar tensor in the crystallographic BZ are summed up in.[4] Here, we give the formulas for the magnetic BZ.

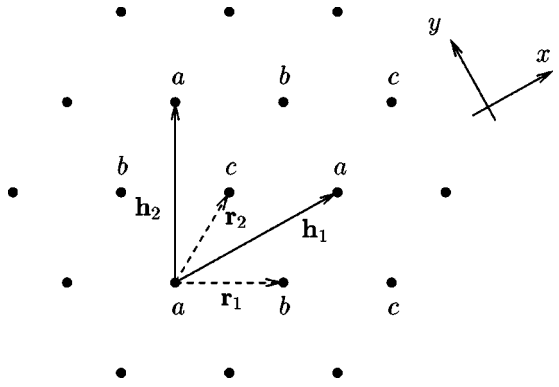

FIG. 23. Parametrization of the lattice.

When we performed ground-state calculations for a general six-sublattice model, we had a basis with six spins and replicated this cell to build up the lattice (see Figs. 13, 23). To find the classical ground state energy of this structure, we parametrize one of the six sublattices with vectors **h** and the basis cell with vectors $\mathbf{r}_a$ to $\mathbf{r}_f$.

Here sublattice *A* is parametrized in a coordinate system, which is rotated by 30° to the crystallographic one

$$\mathbf{h}_1 = a(\sqrt{3},0,0), \quad \mathbf{h}_2 = \frac{a}{2}(\sqrt{3},1,0), \quad \mathbf{h}_3 = c(0,0,2) \tag{B1}$$

and the vectors describing the basis are given by

$$\mathbf{r}_a = (0,0,0), \quad \mathbf{r}_b = \frac{a}{2}(\sqrt{3},-1,0), \quad \mathbf{r}_c = \frac{a}{2}(\sqrt{3},1,0),$$

$$\mathbf{r}_d = c(0,0,1), \quad \mathbf{r}_e = \frac{a}{2}\left(\sqrt{3},-1,2\frac{c}{a}\right), \quad \mathbf{r}_f = \frac{a}{2}\left(\sqrt{3},1,2\frac{c}{a}\right). \tag{B2}$$

Here *c* is the distance of neighboring lattice sites along the chain direction and *a* the one within basal planes. To include the full three-dimensional dipolar energy, we need the contribution of the dipolar energy from the interaction of sublattice a with sublattices $a-f$, the interaction of sublattice *b* with all other sublattices and so on. This means, that we have to calculate Fourier transforms with respect to a linear combination of two basis vectors. The dipolar tensor splits up in two contributions on the direct lattice and one for the indirect lattice (Ewald-summation technique[16,17]) and finally reads

$$A^{\alpha\beta}_{\mathbf{q},ab}\frac{a_3}{G} = \begin{cases} -2\pi\delta_{\alpha\beta}\sum_l{}' \, e^{i\mathbf{q}[\mathbf{x}_l-(\mathbf{r}_a-\mathbf{r}_b)]} \\ \quad \times \varphi_{1/2}\left(\dfrac{\pi}{a_3^{2/3}}|\mathbf{x}_l-(\mathbf{r}_a-\mathbf{r}_b)|^2\right) \\ +4\pi^2 a_3^{-2/3}\sum_l{}' \, e^{i\mathbf{q}[\mathbf{x}_l-(\mathbf{r}_a-\mathbf{r}_b)]} \\ \times[\mathbf{x}_l-(\mathbf{r}_a-\mathbf{r}_b)]_\alpha[\mathbf{x}_l-(\mathbf{r}_a-\mathbf{r}_b)]_\beta \\ \quad \times \varphi_{\frac{3}{2}}^3\left[\dfrac{\pi}{a_3^{2/3}}|\mathbf{x}_l-(\mathbf{r}_a-\mathbf{r}_b)|^2\right] \\ -a_3^{2/3}\sum_{\mathbf{G}} \, (\mathbf{q}+\mathbf{G})_\alpha(\mathbf{q}+\mathbf{G})_\beta \\ \quad \times e^{i\mathbf{G}[\mathbf{x}_l-(\mathbf{r}_a-\mathbf{r}_b)]}\varphi_0\left(\dfrac{a_3^{2/3}}{4\pi}|\mathbf{q}+\mathbf{G}|^2\right), \end{cases} \tag{B3}$$

where $a_3 = 3\sqrt{3}a^2c$ is the volume of the primitive cell of the magnetic sublattice. The components of the dipolar tensor in the magnetic BZ are connected to the ones in the crystallographic BZ. Here we give some of these exact relations:

$$\begin{aligned} 2(A^{11}_{\mathbf{q}_1}-A^{11}_{\mathbf{q}_0}) &= A^{11}_{0,ab}-A^{11}_{0,ae}, \\ 2(A^{22}_{0}-A^{22}_{2\mathbf{q}_4}) &= A^{11}_{0,ab}+A^{11}_{0,ae}, \\ 2(A^{22}_{0}+2A^{22}_{2\mathbf{q}_4}) &= A^{11}_{0,ad}+A^{11}_{0,aa}, \\ 2(A^{11}_{\mathbf{q}_1}+2A^{11}_{\mathbf{q}_0}) &= A^{11}_{0,aa}-A^{11}_{0,ad}. \end{aligned} \tag{B4}$$

APPENDIX C: POINTS IN THE BRILLOUIN ZONE

In this appendix we compile the different wave vectors used in the body of the paper. Below each wave vector the points in the Brillouin zone are given, compare Fig. 1.

$\mathbf{q}=0$		$\mathbf{q}_1=(0,0,\pi)$
	$\mathbf{q}_0=\left(\frac{4\pi}{3},0,\pi\right)$	
Γ	H	A
$\mathbf{q}_2=\left(0,\frac{2\pi}{\sqrt{3}},\pi\right)$	$\mathbf{q}_3=\left(\frac{2\pi}{3},\frac{2\pi}{\sqrt{3}},\pi\right)$	$\mathbf{q}_4=\left(\frac{4\pi}{3},0,0\right)$
L	H'	K
$\mathbf{q}_5=\left(\pi,\frac{\pi}{\sqrt{3}},\pi\right)$	$\mathbf{q}_6=\left(\pi,-\frac{\pi}{\sqrt{3}},\pi\right)$	$\mathbf{q}_7=\left(0,\frac{2\pi}{\sqrt{3}},0\right)$
L'	L''	M

[1] A. Skjeltorp and D. Sherrington, *Dynamical Properties of Unconventional Magnetic Systems* (Kluwer Academic, Dordrecht, 1998).
[2] H. Diep, *Magnetic Systems with Competing Interactions* (World Scientific, Singapore, 1994).
[3] E. Frey and F. Schwabl, Adv. Phys. **43**, 577 (1994).
[4] C. Pich and F. Schwabl, Z. Phys. B: Condens. Matter **104**, 165 (1997).
[5] C. Pich and F. Schwabl, Phys. Rev. B **47**, 7957 (1993).
[6] F. Haldane, Phys. Rev. Lett. **50**, 1153 (1983).

[7] M. Steiner and H. Mikeska, Adv. Phys. **40**, 191 (1991).
[8] M. Collins and O. Petrenko, Can. J. Phys. **75**, 605 (1997).
[9] G. McPherson, T. Kistenmacher, and G. Stucky, J. Chem. Phys. **52**, 815 (1970).
[10] C. Pich and F. Schwabl, Phys. Rev. B **55**, 3351 (1997).
[11] H. Shiba and N. Suzuki, J. Phys. Soc. Jpn. **51**, 3488 (1982).
[12] M. Baehr, M. Winkelmann, P. Vorderwisch, M. Steinr, C. Pich, and F. Schwabl, Phys. Rev. B **54**, 12 932 (1996).
[13] H. Kadowaki, K. Hirakawa, and K. Ubukoshi, J. Phys. Soc. Jpn. **52**, 1799 (1983).
[14] P. Santini, G. Fáth, Z. Domański, and P. Erdös, Phys. Rev. B **56**, 5373 (1997).
[15] R. Dietz, L. Walker, F. Hsu, and W. Haemmerle, Solid State Commun. **15**, 1799 (1974).
[16] P. Ewald, Ann. Phys. (Leipzig) **64**, 253 (1921).
[17] L. Bonsall and A. Maradudin, Phys. Rev. B **15**, 1959 (1977).
[18] M. Hummel, C. Pich, and F. Schwabl, J. Appl. Phys. **85**, 5088 (1999).
[19] J. Goodyear and D. Kennedy, Acta Crystallogr., Sect. B: Struct. Crystallogr. Cryst. Chem. **28**, 1640 (1972).
[20] T. Holstein and H. Primakoff, Phys. Rev. **58**, 1098 (1940).
[21] K. Elk and W. Gasser, *Die Methode der Greenschen Funktion in der Festkörperphysik* (Akademie Verlag, Berlin, 1979).
[22] J. Oyedele and M. Collins, Can. J. Phys. **56**, 1482 (1978).
[23] U. Falk, A. Furrer, H. Güdel, and J. Kjems, Phys. Rev. B **35**, 4888 (1987).
[24] B. Gaulin, M. Collins, and W. Buyers, J. Appl. Phys. **61**, 3409 (1987).
[25] L. Heller, M. Collins, Y. Young, and B. Collier, Phys. Rev. B **49**, 1104 (1994).
[26] A. Chubukov, J. Phys. C **21**, L441 (1988).
[27] S. Abarzhi, A. Bazhan, L. Prozorova, and I. Zaliznayak, J. Phys. C **4**, 3307 (1992).
[28] E. Rastelli and A. Tassi, Phys. Rev. B **49**, 9679 (1994).
[29] A. Abanov and O. Petrenko, Phys. Rev. B **50**, 6271 (1994).
[30] P. Santini, Z. Domański, J. Dong, and P. Erdös, Phys. Rev. B **54**, 6327 (1996).
[31] M. Zhitomirsky and I. Zaliznyak, Phys. Rev. B **53**, 3428 (1996).
[32] C. Pich and F. Schwabl, J. Magn. Magn. Mater. **148**, 30 (1995).
[33] M. Collins and B. Gaulin, J. Appl. Phys. **55**, 1869 (1984).
[34] B. Kotyuzhanskii and D. Nikiforov, J. Phys.: Condens. Matter **3**, 385 (1991).
[35] T. Goto, T. Inami, and Y. Ajiro, J. Phys. Soc. Jpn. **59**, 2328 (1990).
[36] M. Hummel, C. Pich, and F. Schwabl, cond-mat/9703218 (unpublished).